

Hydrofoil Design and Construction



UNIVERSITAT POLITÈCNICA DE CATALUNYA
BARCELONATECH

Escola Superior d'Enginyeries Industrial,
Aeroespacial i Audiovisual de Terrassa

Author: Pol Bernad Serra

Director: Aleix Báez

UPC ESEIAAT

Grau en Enginyeria en Vehicles Aeroespacials

Delivery Date: 10th of June, 2019

Abstract

This TFG project reports the design and prototyping of a surf hydrofoil. The hydrodynamic design has been done with a NASA's open source software Open VSP together with a simulation platform on Simulink. Some geometries have been designed, 3D printed and tested in a scale bench pulled from a boat. The best geometry has been constructed with glass fibre and steel and tested in real scale. All the work has been done at home with own elaborated machines like a 3D printer or a CNC.

Table of Contents

1.	Introduction	9
1.1	Aim	9
1.2	Scope	9
1.3	Justification	9
1.4	Background.....	10
1.5	Acknowledgment	11
2.	State of the art	12
3.	Design.....	15
3.1	Objectives and constrains	15
3.2	Methodology	16
3.3	Geometry design.....	17
3.3.1	Alpha	18
3.3.2	Beta	22
3.4	Platform design	26
3.4.1	Solid Block	27
3.4.2	Hydrodynamics Block	28
3.4.3	Control Block	31
3.4.4	The smaller blocks	33
3.5	Geometry comparison.....	34
3.5.1	Alpha	34
3.5.2	Beta	37
3.5.3	Comparison	40
4.	Model	41
4.1	Construction	41
4.1.1	Geometry	42
4.1.2	Surf Board.....	44
4.1.3	Sliding Mass.....	44
4.1.4	Articulated quadrilateral	51
4.2	Tests	53
4.2.1	First test.....	53
4.2.2	Second test.....	53
4.2.3	Third test	54

4.2.4	Fourth test.....	55
4.3	Decision making	56
5.	Real Scale Model	57
5.1	Structural design	57
5.1.1	Internal structure	57
5.1.2	Lifting surfaces	59
5.2	Construction.....	61
5.2.1	Internal Structure	61
5.2.2	Molds.....	63
5.2.3	Lifting surfaces	68
5.2.4	Board	75
5.3	Tests	76
5.3.1	First test.....	76
5.3.2	Second test.....	77
5.3.3	Third test	78
6.	Future work.....	79
7.	Timing.....	79
8.	Conclusions	81
9.	Bibliography	82

List of Figures

Figure 1: Side force and angles diagram	10
Figure 2: Bottom force and angles diagram	11
Figure 3: Hydrofoil 1	12
Figure 4: Hydrofoil 2	12
Figure 5: Hydrofoil 3	13
Figure 6: Hydrofoil 4	13
Figure 7: Hydrofoil 5	14
Figure 8: Design methodology	16
Figure 9: Alpha geometry	18
Figure 10: Alpha Cm	19
Figure 11: Alpha CL	19
Figure 12: Alpha Cn	20
Figure 13: Naca 23012 (Airfoil Tools, 2019)	20
Figure 14: Sweep effect	21
Figure 15: Beta	22
Figure 16: Beta Cm	23
Figure 17: Beta CL	23
Figure 18: Beta Cn	24
Figure 19: ESA40 (Airfoil Tools, 2019)	24
Figure 20: Platform overview	26
Figure 21: Solid block	27
Figure 22: Solid block structure	27
Figure 23: Hydrodynamics block	28
Figure 24: Hydrodynamics structure	28
Figure 25: Coefficients calculator structure	29
Figure 26: Depth effect	30
Figure 27: Control block	31
Figure 28: Control block structure	32
Figure 29: Alpha body angles control off	34
Figure 30: Alpha velocity control off	35
Figure 31: Alpha submergence control off	35
Figure 32: Alpha body angles control on	36
Figure 33: Alpha Velocity control on	36
Figure 34: Alpha submergence control on	37
Figure 35: Beta body angles control off	37
Figure 36: Beta velocity control off	38
Figure 37: Beta submergence control off	38
Figure 38: Beta body angles control on	39
Figure 39: Beta velocity control on	39
Figure 40: Beta submergence control on	40
Figure 41: Scale model test	41
Figure 42: Open VSP geometry	42
Figure 43: Ready to print geometry	42
Figure 44: 3d printed Alpha geometry	42
Figure 45: Surface treatment for gluing	43
Figure 46: Gluing process	43

Figure 47: 3d printed Beta geometry	43
Figure 48: Final Alpha geometry	43
Figure 49: Final Beta geometry	43
Figure 50: Components of the sliding mass system	45
Figure 51: Central piece assembled	45
Figure 52: Central piece printed	45
Figure 53: The final design	46
Figure 54: The first design approach	46
Figure 55: Custom Arduino NANO pcb	47
Figure 56: Connections photo	47
Figure 57: Custom driver pcb	47
Figure 58: Tin channels	47
Figure 59: Failed electronic components	48
Figure 60: Final sliding mass system	49
Figure 61: Final scale model constructed	49
Figure 62: Real model for comparison	50
Figure 63: Render of the model	50
Figure 64: Articulated quadrilateral on a test	51
Figure 65: Articulated quadrilateral build	51
Figure 67: Plastic tub ends joints	51
Figure 67: Aluminium hinge inserts	51
Figure 68: Quadrilateral tip	52
Figure 69: Quadrilateral root	52
Figure 70: Definitive bearings position	52
Figure 71: First bearings position	52
Figure 72: Second test. No tension on the ropes	54
Figure 73: Final internal structure render	57
Figure 74: First central tub wing load diagram	58
Figure 75: First central tub tail load diagram	58
Figure 76: Final central tub wing load diagram	58
Figure 77: Final central tub tail load diagram	58
Figure 78: Tail load diagram	59
Figure 79: Wing load diagram	59
Figure 80: Naca 23015 bending inertia (Online Wing Bending Inertia Calculator, 2019)	60
Figure 81: Ensuring perpendicularity with a machined to square aluminium plate	61
Figure 82: Welded joint	61
Figure 83: The results after the first welding day	62
Figure 84: Finished internal structure	62
Figure 85: Finished wing mold	63
Figure 86: Wing mold render	63
Figure 87: Face operation toolpath	64
Figure 88: Adaptative clearing machining	64
Figure 89: Adaptative clearing toolpath	64
Figure 90: Parallel machining	65
Figure 91: Parallel toolpath	65
Figure 92: Parallel 2 toolpath	65
Figure 93: Contour toolpath	65
Figure 94: Surface finish after treatment	66
Figure 95: Surface finish before treatment	66
Figure 96: Wing mold after varnishing	67
Figure 97: Finished tail mold	67

Figure 98: Perforated polyethylene film	68
Figure 99: Vacuum fridge pump.....	68
Figure 100: Template transferred to the fibre mat.....	69
Figure 101: Paper template.....	69
Figure 102: Plastic adapter for the vacuum tub.....	69
Figure 103: Manual-laying the composite material	70
Figure 104: Resin excess being absorbed by the paper	70
Figure 105: Pressing the vacuum bag to avoid bridging	70
Figure 106: First composite part	71
Figure 107: Checking the wall thickness	71
Figure 108: Leveling the tail	72
Figure 109: Wing joint procedure	72
Figure 110: Tail joint procedure	72
Figure 111: Joint surface problem.....	72
Figure 112: Joint solution	73
Figure 113: Leading edge fibre strip.....	73
Figure 114: Clamping the halves	73
Figure 115: Final result after sanding.....	74
Figure 116: Polyurethane foam fill.....	74
Figure 117: Finished prototype	75
Figure 118: First test.....	76
Figure 119: Second test.....	77
Figure 120: Third test	78
Figure 121: Project charter's Gantt diagram.....	80

List of tables

Table 1: Alpha characteristics	18
Table 2: Beta Characteristics.....	22
Table 3: Solid block inputs and outputs	27
Table 4: Hydrodynamics block inputs and outputs.....	28
Table 5: CL as function of submergence	30
Table 6: Control block inputs and outputs.....	31
Table 7: Model characteristics	50
Table 8: OWA decision making.....	56

List of Abbreviations

CD	Drag coefficient
CY	Sideslip coefficient
CL	Lift coefficient
CI	Rolling moment coefficient
Cm	Pitching moment coefficient
Cn	Yawing moment coefficient
α	Angle of attack
β	Sideslip angle
μ	Velocity roll angle
γ	Velocity pitch angle
χ	Velocity yaw angle
ϕ	Roll angle
θ	Pitch angle
ψ	Yaw angle
δ	Wave slope

1. Introduction

1.1 Aim

The aim of the TFG is to design, build and test a hydrofoil for foil surf. The design will focus on finding a hydrofoil geometry capable to ensure stable and exciting surfing. Some geometries will be built at scale with a 3D printer and tested. Finally, a winning geometry will be built in full scale with composite materials and tested in real conditions. At the end of the project, a hydrofoil prototype will be ready for industrialization.

1.2 Scope

- Understand the differences between a foil working in air and working in water.
- Analyse the state of use of the hydrofoils.
- Understand and model the requirements of surfing hydrofoils.
- Create a simulation platform with Simulink.
- Design several hydrofoil geometries, test on the simulation platform and understand the relations between geometrical parameters and response.
- Build some scale models of the representative geometries with 3D printing.
- Testing of the scale models.
- Define a final hydrofoil geometry.
- Construction of the final prototype with composite materials.
- Test the final prototype in full scale.
- Report the results.
- The project should be environmentally friendly.

1.3 Justification

Hydrofoils are causing a revolution in water sports. In foil surf they allow surfing weaker waves and riding common waves for longer periods. This allows surfing in the Mediterranean coast of Catalonia, and Southern Europe more days of the year. This opens a market opportunity for a design platform to help predicting the behaviour of these devices prior to construction and for the technologies leading to hydrofoil manufacturing at reasonable costs.

I, as an aerospace student with a background in parts construction and with attraction to the sea and sailing would like to take this opportunity to apply my aerospace engineering knowledge to water sports.

1.4 Background

Cavitation

Cavitation is the phenomenon that describes the phase change from liquid to gas of a fluid due to a reduction of the pressure at constant temperature (Eisenberg, 1968). The forming of bubbles affects the flux changing the hydrodynamic forces. When the bubbles collapse, structural erosion and noise are produced. This is one of the reasons why hydrofoil boats have not been taken place over the traditional floating technology. However, in this study cavitation has not been considered because it is a phenomenon which occurs at much higher speed, and thus pressure difference, than foil surfing does (Acosta, 1973).

Depth effect

The depth effect considers the lift reduction due to the proximity of the wing to the water surface. The transition between air and water must have a pressure of 1atm and thus, there is a contour condition at a variable distance, not like in unrestricted airflow (Acosta, 1973). This lift reduction increases when the submergence of the foil reduces and at the surface the lift must be 0. This phenomenon will be considered in the design section as will be later explained.

Foil surf diagrams

In this section, two diagrams are presented to show the hydrodynamic forces and the angles that will be used to compute and project them. The wave has been considered to be a constant slope sea level as it will be explained in detail in the platform design section.

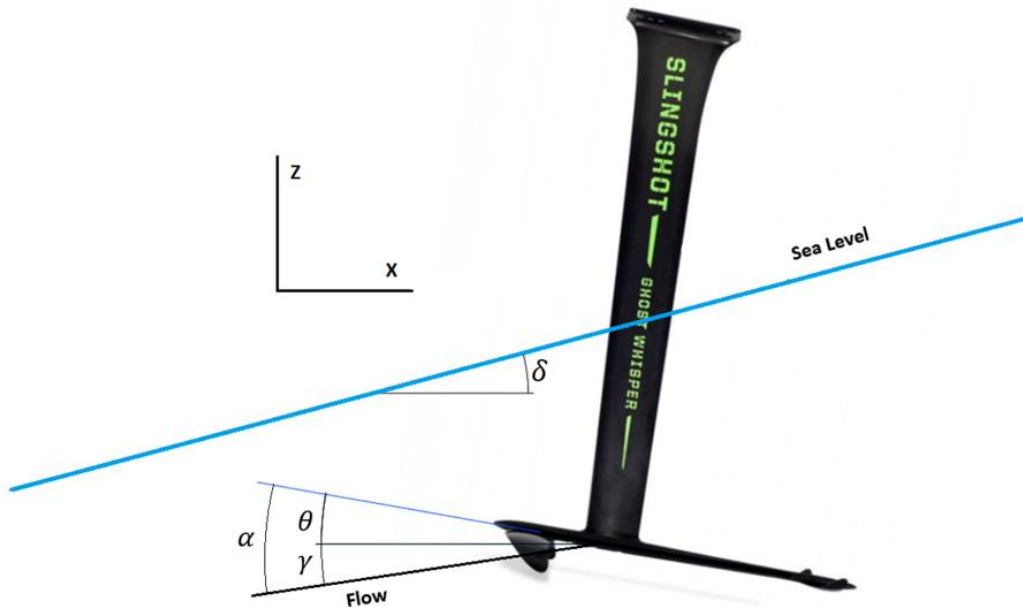


Figure 1: Side force and angles diagram



Figure 2: Bottom force and angles diagram

1.5 Acknowledgment

This project would not be possible without the support of a lot of people which have helped me throw the whole process.

First, I would like to thank my family because they have given me their support and ideas to constantly upgrade the work done. They have also taken care of the entire cost of the elaboration of this project.

Secondly, I would like to acknowledge my uncle who has also helped me with the welding process. I would also like to thank the local metal worker *Josep Vidal* and the local carpenter *Fustes Martínez* who have supplied material without any cost.

Finally, and not less important, I would like to thank the director of this project, Aleix Bález, who has always guided me since the first day and has shown interest in every step of the project.

I would like to thank you all because without you this project would not have been possible.

2. State of the art

This section describes the actual technology used in the industry of foil surf.

Slingshot 2019 Hover Glide Fsurf



This hydrofoil mast and fuselage are made of aluminium and its wing and tail are made of composite material. The mast is 61cm long, the aspect ratio 3.7, the surface area is 1534 cm² and the wingspan is 77cm. Its price is 1170€.

Figure 3: Hydrofoil 1

Naish 2019 Foil Surf Thrust XL



The fuselage and the vertical support are also made of aluminium. The wing and the tail are made of monocoque carbon and glass fibre with a foam core. The mast is 55cm long, the aspect ratio is 4.75, the wingspan is 86cm and the surface is 1572cm². The price for this hydrofoil is 1470€.

Figure 4: Hydrofoil 2

Ride Engine 2019 Futura Sup Foil



Figure 5: Hydrofoil 3

This foil construction consists again of aluminium fuselage and mast and carbon fibre reinforcement plastic wings. Its mast is 61cm high, the aspect ratio is 3.3, the surface area is 2066cm² and its wingspan is 84cm. the price of this foil is 1040€.

Naish 2019 Foil Wind Thrust



Figure 6: Hydrofoil 4

This foil is not for wave surf but for windsurf. Its construction is like the others seen before, aluminium fuselage and mast and composite material wings. Its mast is 70cm long, its aspect ratio is 3.46, the wingspan is 65cm and its surface area is 1220cm². Its price is 1360€.

Fanatic Aero Sup Foil 2000 Long Fuselage 2019



This is a wave surf hydrofoil and its construction is like the others'. Its fuselage and mast are made of aluminium and the wings are made out of carbon composite material. The mast is 75cm long, the wingspan is 99cm and the surface area is 2000 cm². The selling price is 1350€.

Figure 7: Hydrofoil 5

From the state of the art it can be seen that the current technology for the foil surf uses the same construction methods, aluminium fuselage and mast and composite material wings. The surf hydrofoils have a surface area between 1500 and 2000 cm², a wingspan between 60 and 100cm, a variable aspect ratio between 3 and 5 and a mast length between 55 and 75cm. The average price is above 1000€. All the information for the elaboration of the state of the art has been obtained from (B3 Proshop, 2019).

3. Design

This section describes the design process and final geometry of the hydrofoil.

3.1 Objectives and constraints

The objectives that need to be accomplished are:

- Develop a hydrofoil which is stable enough to be ridden by a beginner.
- The hydrofoil should lift 80Kg at 6knts.
- The design should allow the construction to be done at home with the tools and machines available.
- The wing structure will be made of composite material and the internal structure of stainless-steel.
- The whole surf should weight under 20kg because it has to be carried by only one person.
- It should allow surfing in low waves condition

The constraints that limit the design are:

- The 3D printer maximum print dimensions which restrict the size of the scale model.
- The CNC maximum dimensions which restricts the molds dimensions.
- The budget.
- The deadline.

3.2 Methodology

The hydrodynamic design started with generating and optimizing different geometries with an open source software Open VSP. To do so, different parameters of the geometry were changed and then the coefficients which describes the flight behaviour were computed again. The software uses a Vortex Lattice Method (VLM) to compute the coefficients. The computation time for each iteration took about 2min. Once the static stability was accomplished, the dynamic stability was studied with an own elaboration platform on Simulink. To do so, all the coefficients for all the possible angles were computed by the Open VSP. This process took about 1:30h. Then, the results were imported into the Simulink Platform which took about 10 seconds to compute the dynamic behaviour. Finally, this platform was used to compare the different designed geometries. In Addition, a scale test is also used to choose the best geometry. The testing requires 3D printing the geometry and all the test operation. This process is much slower. The following image shows a block diagram of the design structure:

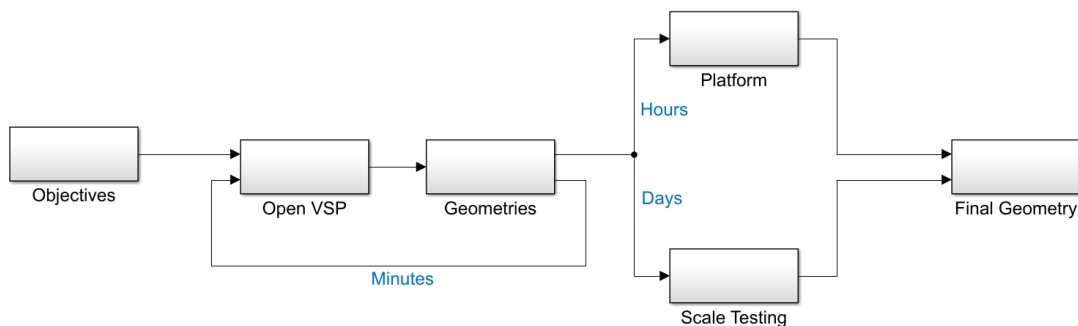


Figure 8: Design methodology

3.3 Geometry design

This section describes the design of the geometry using the NASA's open source software Open VSP. The design should be done efficiently since the optimization of the geometries needs a lot of different iterations. So, the computation time required for each calculation should be short. Every time the geometry is changed, the software needs to recalculate all of the coefficients which takes about 2min.

For this design process there have been three curves considered for each iteration:

- Cm-alpha: this curve represents the pitching moment coefficient as function of the angle of attack. For the plane to be stable the slope of this curve must be negative. This means that when a perturbation, for example, increases the angle of attack, the moment resultant should be more negative than before because this means the plane is trying to minimize this increase of alpha. The other important design aspect is the 0-moment angle. This angle is where the geometry will try to equilibrate itself. The position of the centre of mass has a major effect over this curve. This is the principal problem of this design, the centre of mass is located at 1.5m over the plane's wing, which is more than its wingspan. The tail volume is another key factor for design because it changes the slope of the curve and also changes the cut-off point. The angle of attack of the wing and the tail can be also used in addition with the wing's planform. The profile used also affects to the moment distribution.
- CL-alpha: this curve represents the lift coefficient as function of the angle of attack. The before commented 0-moment alpha should have enough lift to maintain a flight at a reasonably low speed. The profile and the wing's angle of attack have a huge effect over this curve.
- Cn-beta: this curve represents the yawing moment coefficient as function of the angle side-slip angle. This curve is used to size the vertical stabilizer and its slope should also be negative to dissipate perturbations.

The first idea was to optimize 4 different type of geometries: conventional, biplane, flying wing and canard. The optimization was made by proposing a geometry and then changing parameters like its wingspan, sweep or chord distribution and computing again each time until obtaining the desired results; all this process was made with the software Open VSP. However, after the first iterations of the design it was clear that the cm-alpha was the principal problem because of the before commented height of the centre of mass. It was very difficult to obtain a negative slope and also a positive lift angle of equilibrium. For this reason, the canard geometry which are the more difficult geometries to stabilise was discarded. As the one wing geometries were already giving enough lift, the biplane was also discarded because of its constructive complexity. So, the remaining type of geometries were the conventional and the flying wing.

3.3.1 Alpha

The alpha geometry is the conventional design. One major advantage over the flying wing is that the major font of lift, the wing, is detached from the font of stability, the tail. This made possible to change the equilibrium angle or the slope of the Cm-alpha graph without compromising the lift too much. For this case, there were some construction limitations. In order to fit in two pieces inside the CNC machine, the wingspan could not be bigger than 1m and the tail wingspan should be 0.5m to fit in one piece. The resultant geometry after all the iterations was the following:

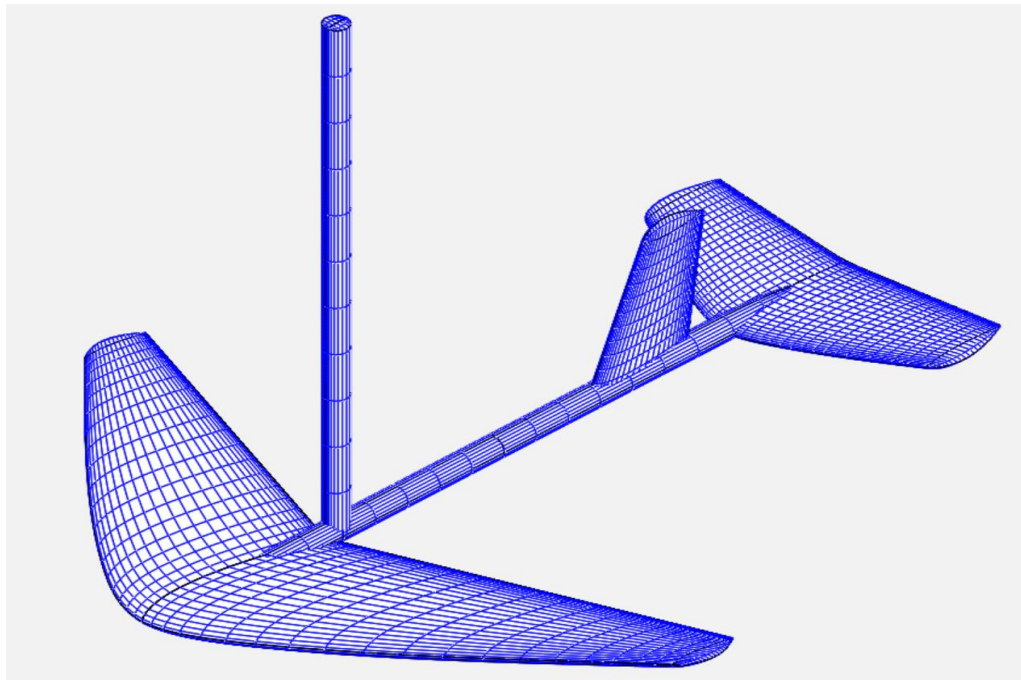


Figure 9: Alpha geometry

Next, a table with the geometry properties:

Property	Value
Wingspan	1m
Tailspan	0.5m
Wing surface	0.19 m ²
Aspect ratio	5.26
Wing Foil	Naca23015-Naca23012
Tail foil	Naca0012
Tail volume coefficient	1.67
Angle of equilibrium	1°
CL at equilibrium	0.27
Sweep at 0.25 chord	35°
Twist	0°
Wing's angle of attack	3°
Tail's angle of attack	-2°
Cn-alpha slope	-0.005
CoM X position from leading edge	-0.05 m

Table 1: Alpha characteristics

Next, the three before commented graphs are presented:

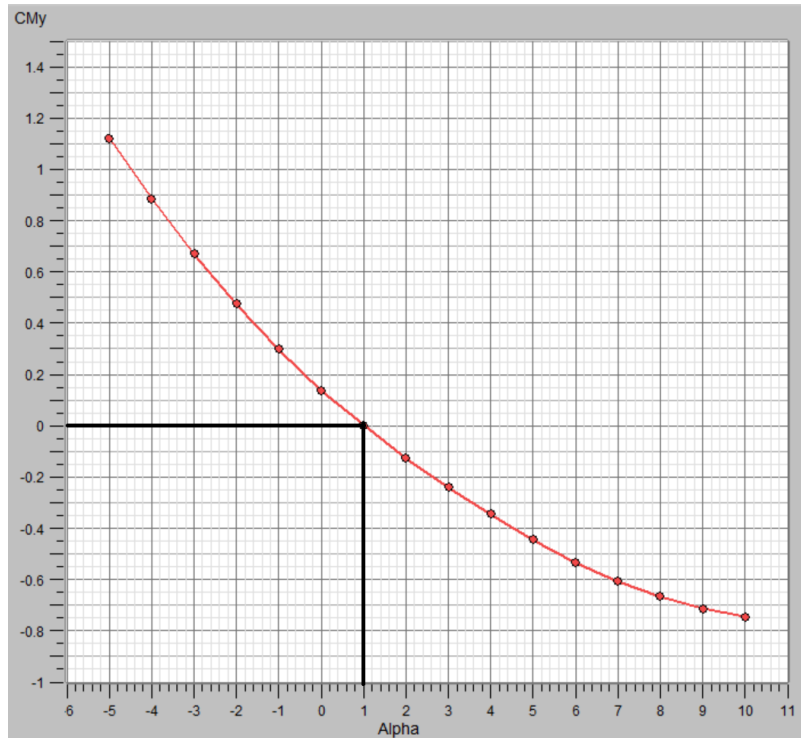


Figure 10: Alpha C_M

As it can be seen, the equilibrium angle is 1° and the whole slope of the graph is negative.

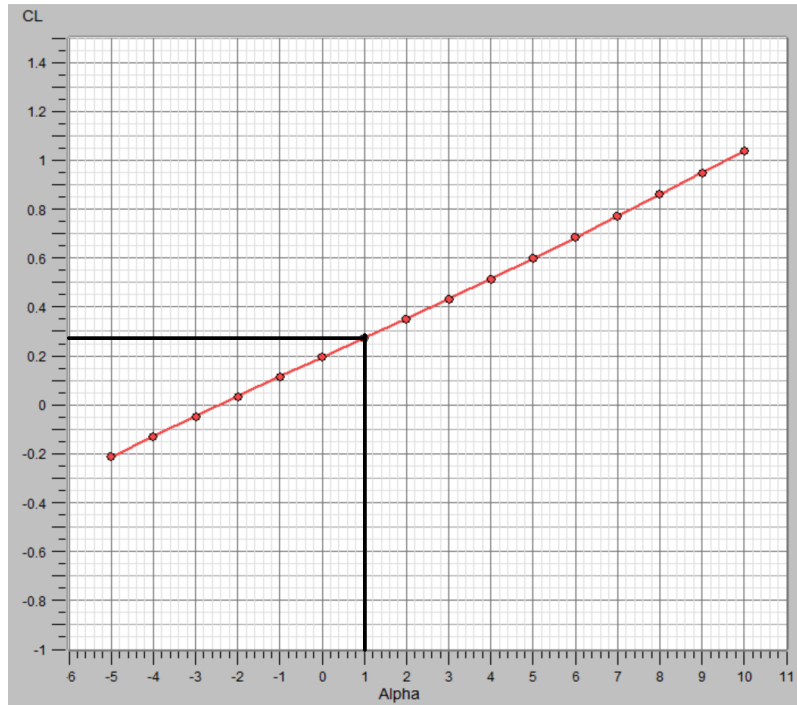


Figure 11: Alpha CL

In this graph it can be observed that at 1° the CL is equal to 0.27.

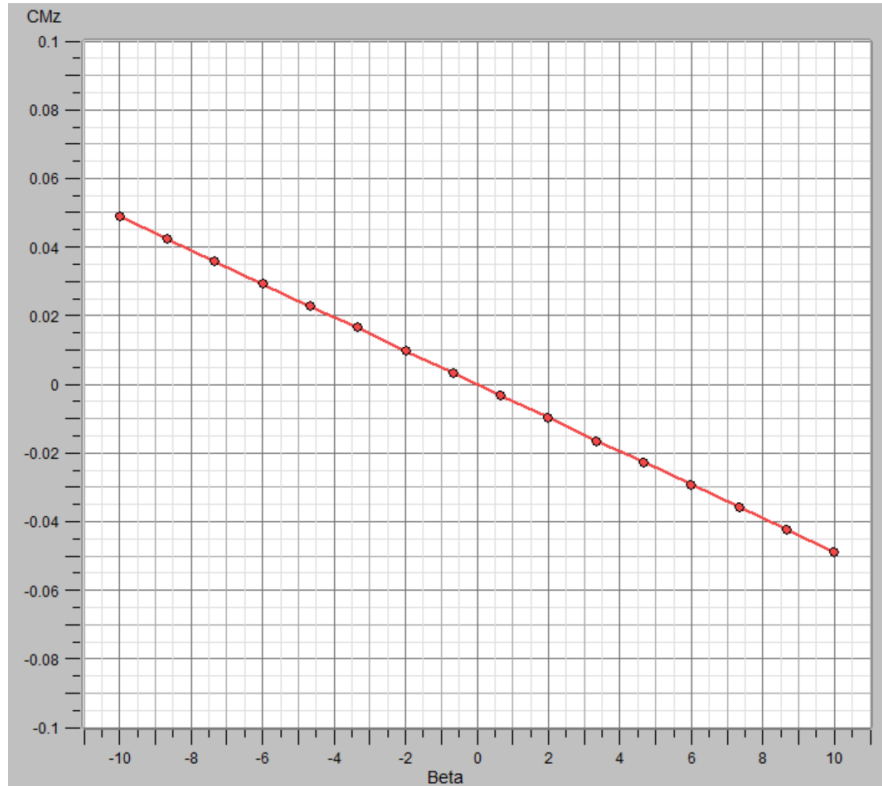


Figure 12: Alpha Cn

It can be extracted from this graph that its slope is -0.005.

As it can be seen in the table, the root foil has a 15% and a 12% thickens at the tip. This is done for structural proposes. It can also be seen that the tail volume coefficient is 1.67 which is much bigger than a regular plane which normally have between 0.3 and 0.6 (Basic Aircraft Design Rules, 2019). This is because the height of the centre of mass need a big tail to counter its unstable moment when pitching. The different angle of attack between wing and tail also made possible to obtain the 1° angle of equilibrium. The foil Naca23012 has given good results because despite of not being the most lift producer, its moment is also low and in combination is the one that offered more lift at its equilibrium angle, 0.27. This means that the required speed is (Franchini & López, 2011):

$$v = \sqrt{\frac{Lift}{\frac{1}{2} \cdot \rho \cdot S_{ref} \cdot CL}} = \sqrt{\frac{800N}{\frac{1}{2} \cdot \frac{1000kg}{m^3} \cdot 0.19m^2 \cdot 0.27}} = 5.6m/s$$

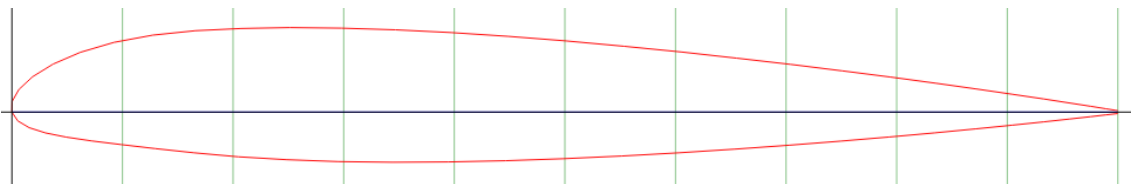


Figure 13: Naca 23012 (Airfoil Tools, 2019)

It is important to point that the sweep helped on the C_m graph, without it the equilibrium point was at the largest angles of attack and the slope it was already positive, making an unstable point of equilibrium. The next figure shows the comparison between C_m of an early design, the left one had sweep and the right one did not have:

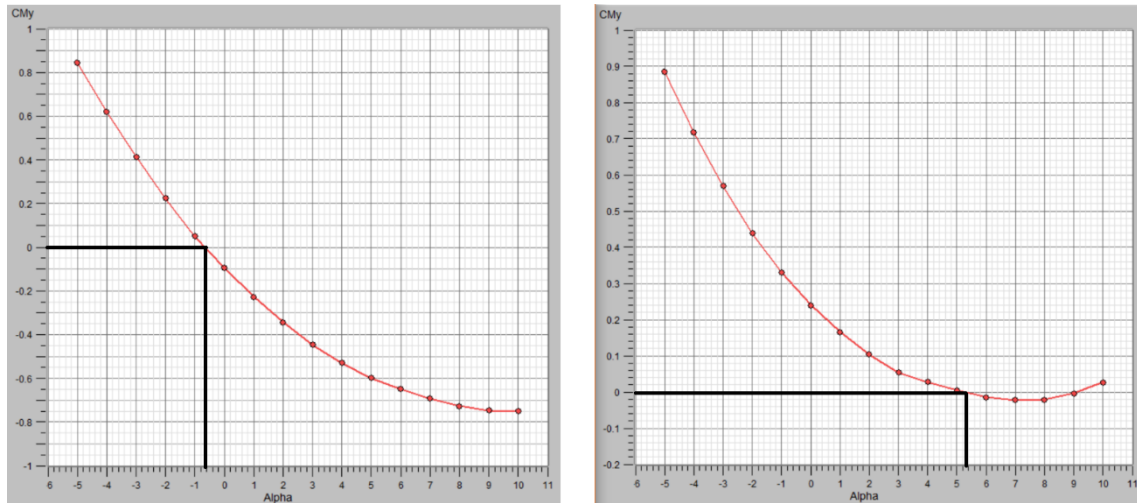


Figure 14: Sweep effect

As it will be explained later, for constructive reasons the 3d printed design and the real scale model are not exactly the same, but the only change is in the vertical support and stabilizer.

3.3.2 Beta

The Beta geometry is the flying wing design. The major advantage of this design is the simplicity. There are no tail and fuselage, so the efficiency is normally better than the conventional designs. However, the lack of tail proposes a difficult challenge to develop a stable geometry with the centre of mass at that high. The size restrictions for this design was that the wing should fit in three parts on the CNC machine, so the maximum wingspan or longitudinal length should be 1.5m. The following image shows the result of the different design iterations:

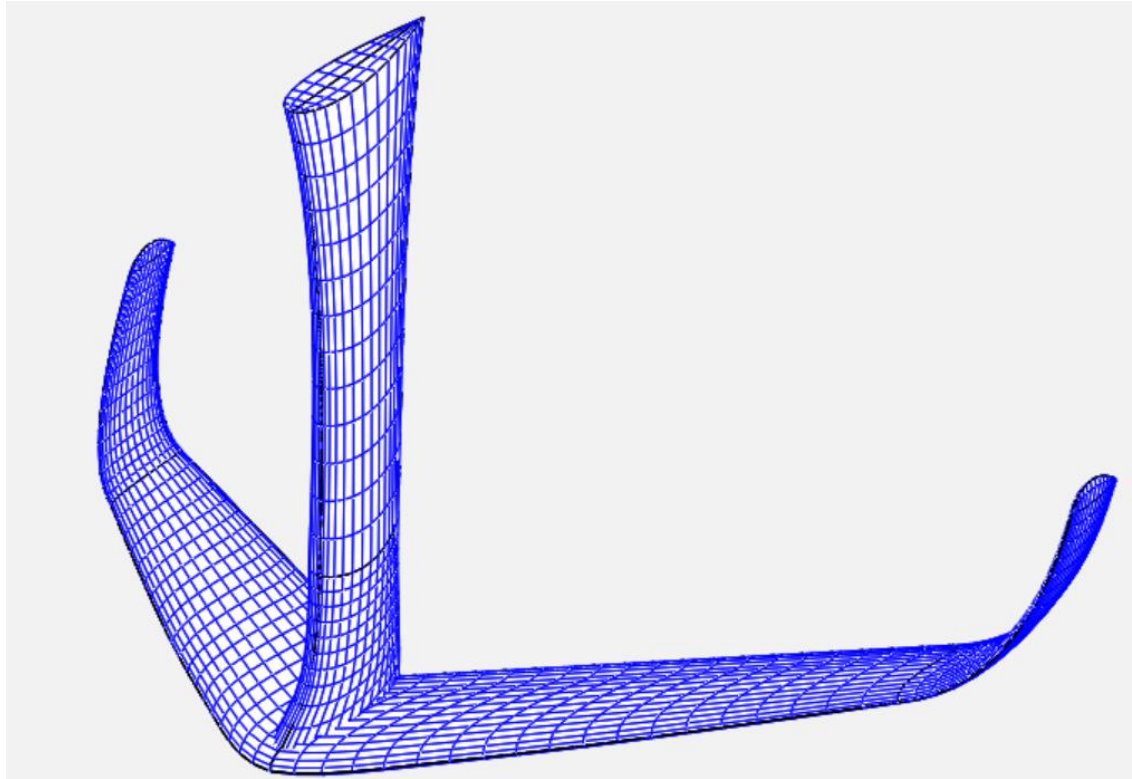


Figure 15: Beta

Next, a table with the geometry properties:

Property	Value
Wingspan	1.3m
Wing surface	0.23 m ²
Aspect ratio	7.35
Foil	ESA40
Angle of equilibrium	0.2°
CL at equilibrium	0.06
Sweep at 0.25 chord	45°
Twist	-5°
Wing's angle of attack	3°
Cn-alpha slope	-0.011
CoM X position from leading edge	-0.05 m

Table 2: Beta Characteristics

Next, the three before commented graphs are presented:

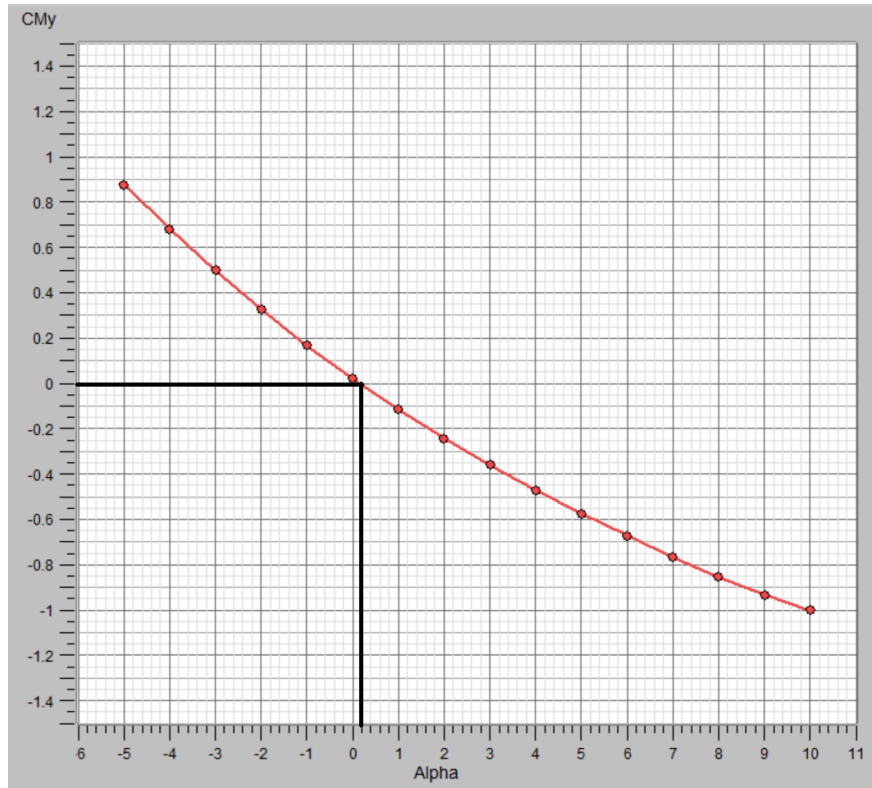


Figure 16: Beta CM

As it can be seen, the equilibrium angle is 0.2° and the whole slope of the graph is negative.

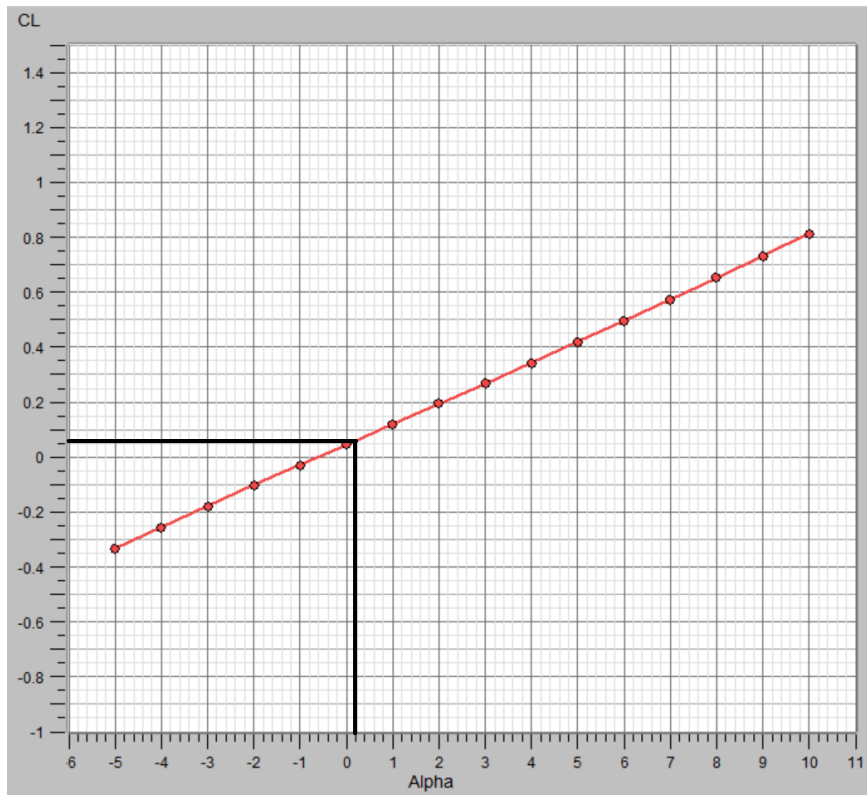


Figure 17: Beta CL

In this graph it can be observed that at 0.2° the CL is equal to 0.06.

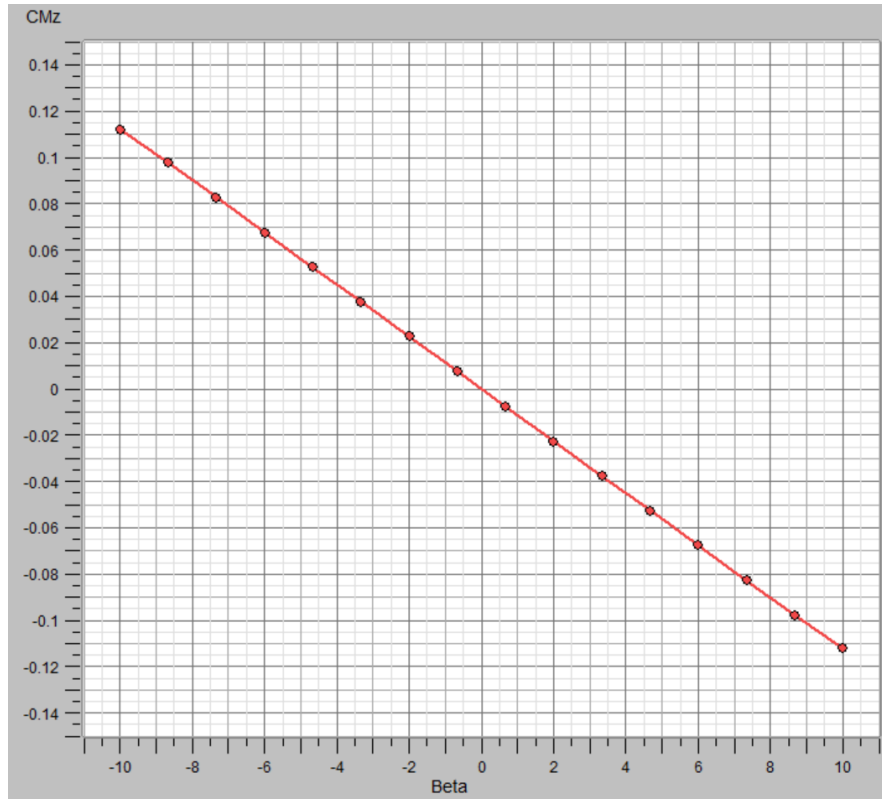


Figure 18: Beta Cn

It can be extracted from this graph that its slope is -0.011.

In the flying wing geometry design there is an essential component, the profile. A regular airfoil has negative moment which means that the tendency is to pitch down. In a regular geometry this effect is counter by the tail. In a flying wing there is no tail so the profile needs to have a moment equal to zero or even positive. These type of airfoils are called reflex. For this study case a regular reflex airfoil was not enough again because of the centre of mass position. The profile selected is the ESA40 which has an average Cm of +0.04. The problem with this type of profiles is that the more Cm they have the less lift is produced.

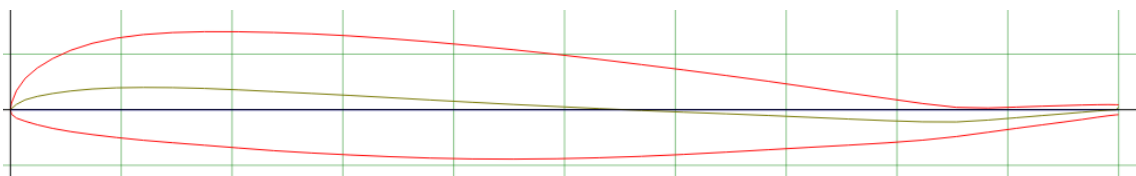


Figure 19: ESA40 (Airfoil Tools, 2019)

However, the airfoil is not the only solution needed to develop a stable tail-less plane. The wing needs to have sweep. In this case, 45°. In addition, to counter the negative moment the wing also has negative twist or wash-out. This lowers the lift produced by the most delayed part of the wing or even it makes it negative. This helps to pitch up. In this case -5° were given to the tip of the wing. However, this technique also reduces the global lift so an equilibrium needs to be found. Lastly, the winglets are necessary not for aerodynamic efficiency but for yaw stability acting as vertical stabilizers.

The final geometry has optimized till obtaining a CL of 0.06 at its equilibrium angle. This means that the required speed is:

$$v = \sqrt{\frac{Lift}{\frac{1}{2} \cdot \rho \cdot S_{ref} \cdot CL}} = \sqrt{\frac{800N}{\frac{1}{2} \cdot \frac{1000kg}{m^3} \cdot 0.23m^2 \cdot 0.06}} = 10.8m/s$$

3.4 Platform design

The Simulink platform is a comparative tool that can compute the dynamic behaviour of a surf hydrofoil with different geometries. It considers the depth effect and a human controlled response.

The Simulink model is divided in 3 main blocks which are connected together:

- Solid
- Hydrodynamics
- Control

There are 4 smaller blocks that feed the main blocks:

- Angles transformation
- Geometry
- Summation
- Initial Conditions

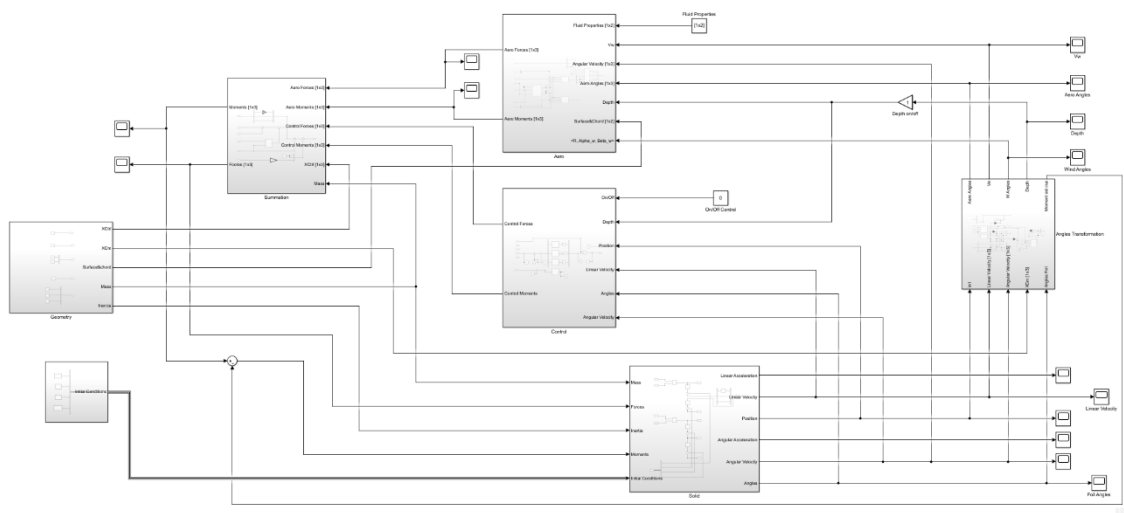


Figure 20: Platform overview

3.4.1 Solid Block

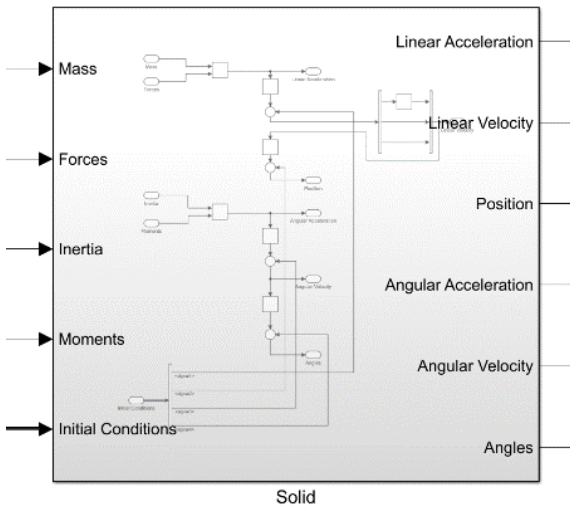


Figure 21: Solid block

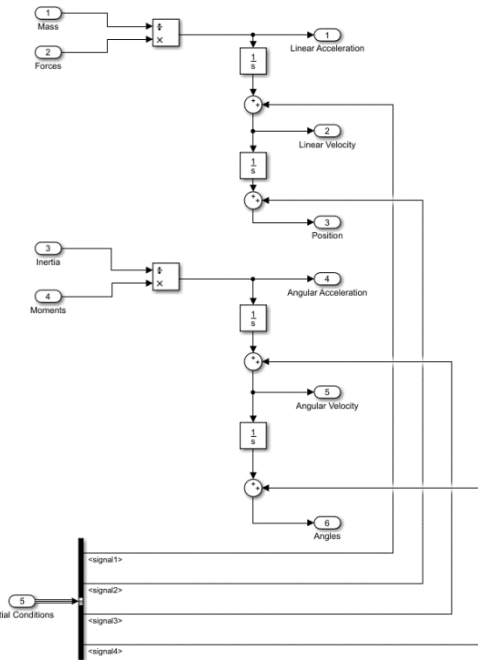


Figure 22: Solid block structure

The solid block task is to compute the dynamic behaviour assuming that the ship is a rigid solid. All the parameters are computed using an inertial reference frame.

There are 2 equations that need to be solved (Gómez & Pérez, 2012):

$$F = m \cdot a$$

$$M = I \cdot \Omega$$

Once the linear and angular accelerations are computed, they are integrated to obtain velocities. Then, the initial velocities from the initial conditions block are added. After that, the velocities are integrated to obtain position and angles. The initial position and angles are also added to the computed values.

The inputs and outputs of the block are the following:

Inputs	Outputs
Mass	Linear Acceleration
Forces	Linear Velocity
Inertia	Position
Moments	Angular Acceleration
Initial conditions	Angular Velocity
	Angles

Table 3: Solid block inputs and outputs

3.4.2 Hydrodynamics Block

The hydrodynamics block task is to compute the static forces and moments produced by the hydrofoil inside the water.

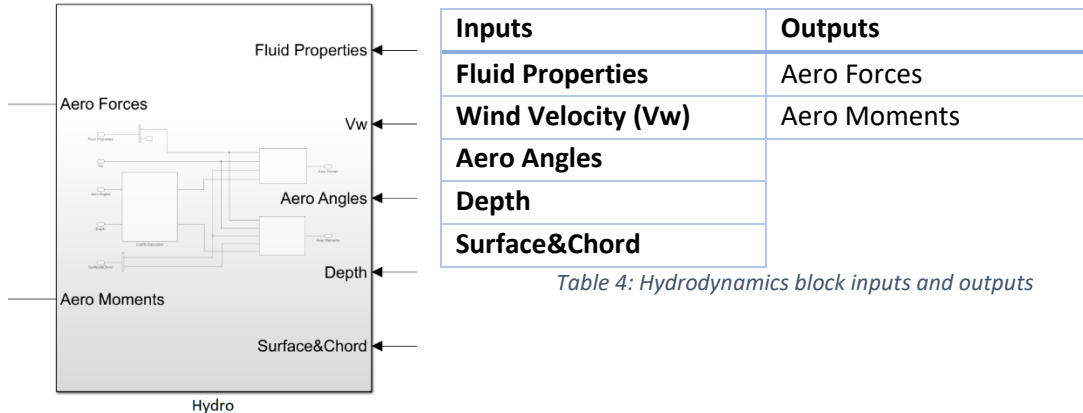


Figure 23: Hydrodynamics block

The main equations that need to be solved in this block are:

$$F = \frac{1}{2} \rho \cdot v_w^2 \cdot S_{ref} \cdot Coeff$$

$$M = \frac{1}{2} \rho \cdot v_w^2 \cdot S_{ref} \cdot C_{ref} \cdot Coeff$$

The density ρ , the wind velocity v_w , the reference surface S_{ref} and the reference chord C_{ref} are inputs of the block. So, the only variables that need to be computed in this block are the 3 force coefficients CD, CY, CL and the 3 moment coefficients Cl, Cm, Cn . This can be seen in the following image:

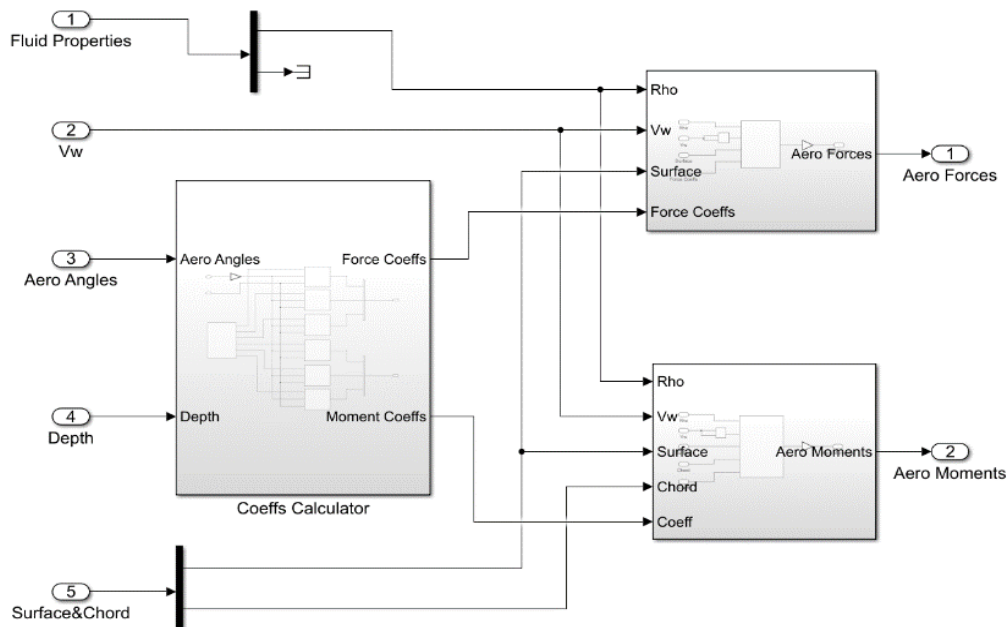


Figure 24: Hydrodynamics structure

In order to compute the coefficients, this block imports data from a NASA's aerodynamics open source software: OpenVSP. This data is imported to Matlab where is selected and organized in a matrix which will be used by Simulink. Then the hydrodynamic block can compute the coefficients as function of α and β and interpolate when it's needed.

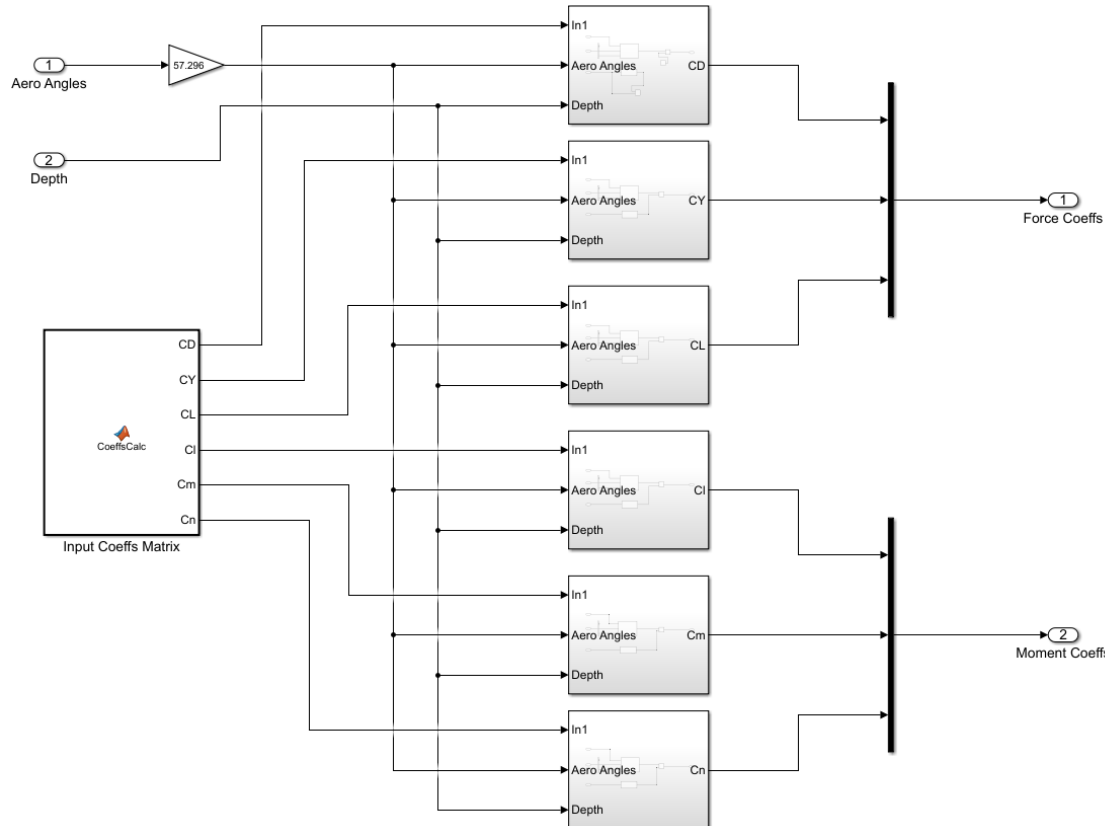


Figure 25: Coefficients calculator structure

In addition, in this block is where the depth effect is considered. This phenomenon reduces the hydrodynamic forces the closer the hydrofoil gets to the water surface. To model this situation 2 identical wings with a symmetrical foil were positioned at a variable vertical distance. The upper wing had $\alpha = -3^\circ$ and the lower one $\alpha = +3^\circ$. The non-variable pressure line is located in between the wings. Having the lift and half the distance between the two wings is possible to adjust a function that describes the forces as function of the submergence. It is important to impose 0 hydrodynamic forces value when the hydrofoil is out of the water. This effect was studied using another open source aerodynamic software called XFLR-5.

The aerodynamic block is now able to compute the forces and moments produced by the hydrofoil in wind reference frame so an Euler angles transformation will be applied in the summation block.

Height	CL	CL Norm
0,010	0,01	0,015
0,250	0,444	0,663
0,050	0,488	0,728
0,100	0,548	0,818
0,250	0,623	0,930
0,500	0,657	0,981

Table 5: CL as function of submergence

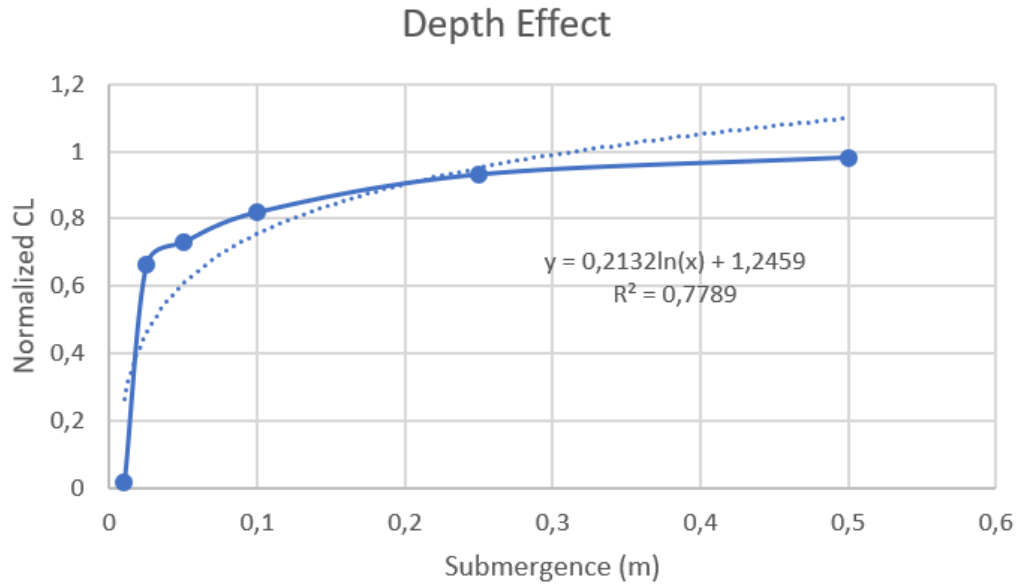


Figure 26: Depth effect

3.4.3 Control Block

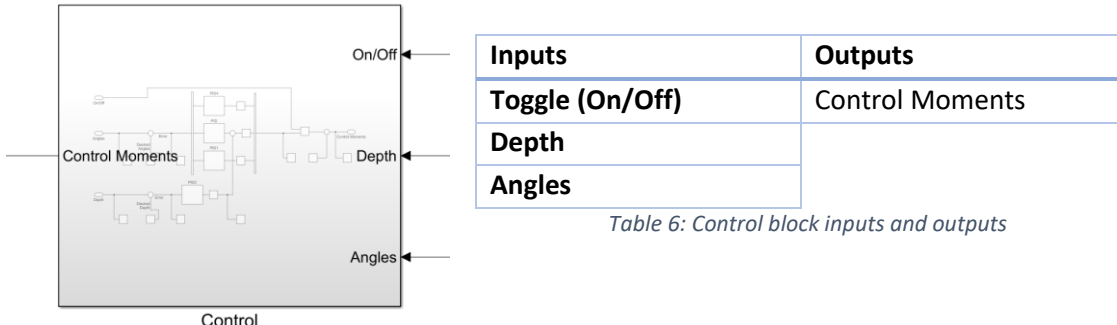


Figure 27: Control block

The control block task is to mimic the response of a person who is over the surf board and tries to stabilize it.

In order to recreate the response of a person, a negative feedback is implemented. The desired angular position is imposed, and the actual angle of the foil is subtracted. The result is the error between the premise and the signal. Then, a PID can be applied to that error in order to create a response against fluctuations. However, the human response is not immediate, there is a delay; the human response is about 0.25 seconds (Human Benchmark, 2019). So, all PID have a 0.25s delay. Furthermore, the person over the surf board is able to produce limited torque. These torque limitations have considered different conditions for each direction:

- Pitch (Y axis): the feet are 0,5m separated and the 620N of weight can be located at the right or left foot completely, so:

$$M = F \cdot d = 620 \cdot \frac{0.5}{2} = \pm 155 Nm.$$

- Roll (X axis): the feet are 0,25m long and the weight can be located at the tip or at the heel, so: $M = F \cdot d = 620 \cdot \frac{0.25}{2} = \pm 77.5 Nm.$
- Yaw (Z axis): the yaw moment comes from inertial rotation forces of the whole body. This means the torque is not sustained on time. This makes it difficult to model so, a quarter of the maximum Roll moment has been assumed to be the maximum value $M = 20 Nm.$

There is another PID for recreating the will of maintaining a constant height above the water surface which is the same as a constant depth. It follows the same negative feedback structure before explained. This moment is added to the pitching torque.

The constants KP, KI and KD, which multiplies the proportional, integral and derivative parts of the PID respectively, is what an experienced hydrofoil surfer would be adjusting in order to respond accurately to perturbations. In this study, the constants have been tuned iteratively comparing the different responds obtained.

Finally, in this image it can be seen the internal structure of the control block:

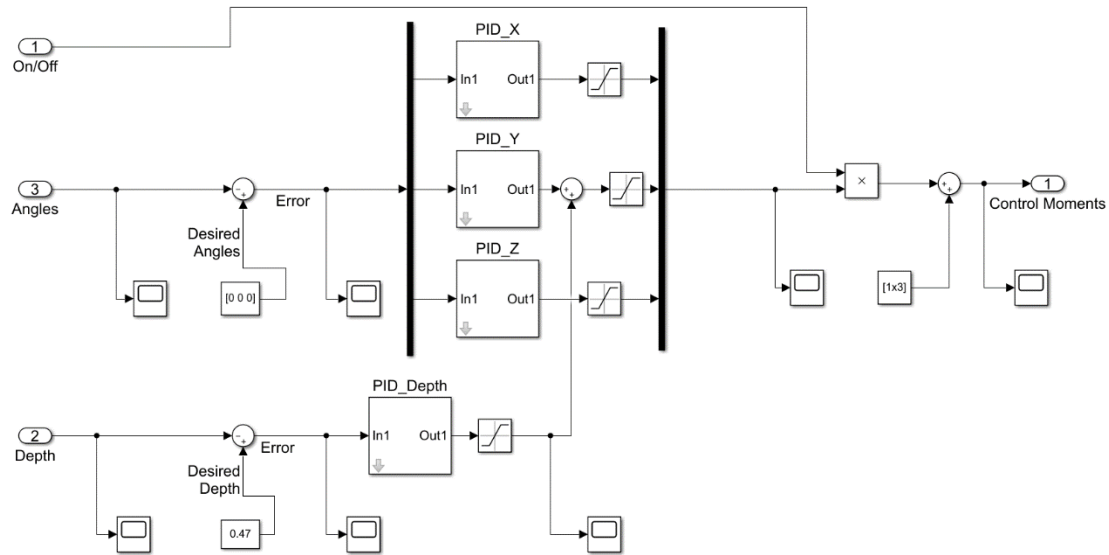


Figure 28: Control block structure

3.4.4 The smaller blocks

There are 4 smaller blocks that feed the main 3 which are:

- Angles transformation: in this block is where all the different angles are computed in the different reference frame. There are three types: the angles of the wind with respect to ground, the angles of the wind with respect to the body and the angles of the body with respect to ground. In this block is where the depth is also computed assuming that the wave has a certain slope.
- Geometry: this block is where properties needed for other blocks such as mass, inertia or the position of the centre of mass are introduced.
- Summation: in this block is where the forces and moments coming from the hydrodynamic and control blocks are added. Then, an Euler transformation is needed to pass from wind reference, where the hydrodynamic forces and moments are referenced to, to ground reference (Gómez & Pérez, 2012).
- Initial Conditions: the initial velocity and position are introduced in this block. This can be used to simulate perturbations setting the initial pitch angle position to, for example, 5°.

3.5 Geometry comparison

In this section is where the geometries are introduced in the Simulink platform and their results are compared. Three graphs are presented for each study case: body angles, the velocity and the submergence of the wing. All these graphs are function of the time in seconds. To simulate perturbations, the initial angle $\theta = -0.2 \text{ rad}$ and the initial angle $\psi = 0.2 \text{ rad}$.

3.5.1 Alpha

Alpha is able to ride a wave of at least $\delta = 10^\circ$ of inclination. The following results were obtained with the control turned off, which means the rider do not react to the perturbations:

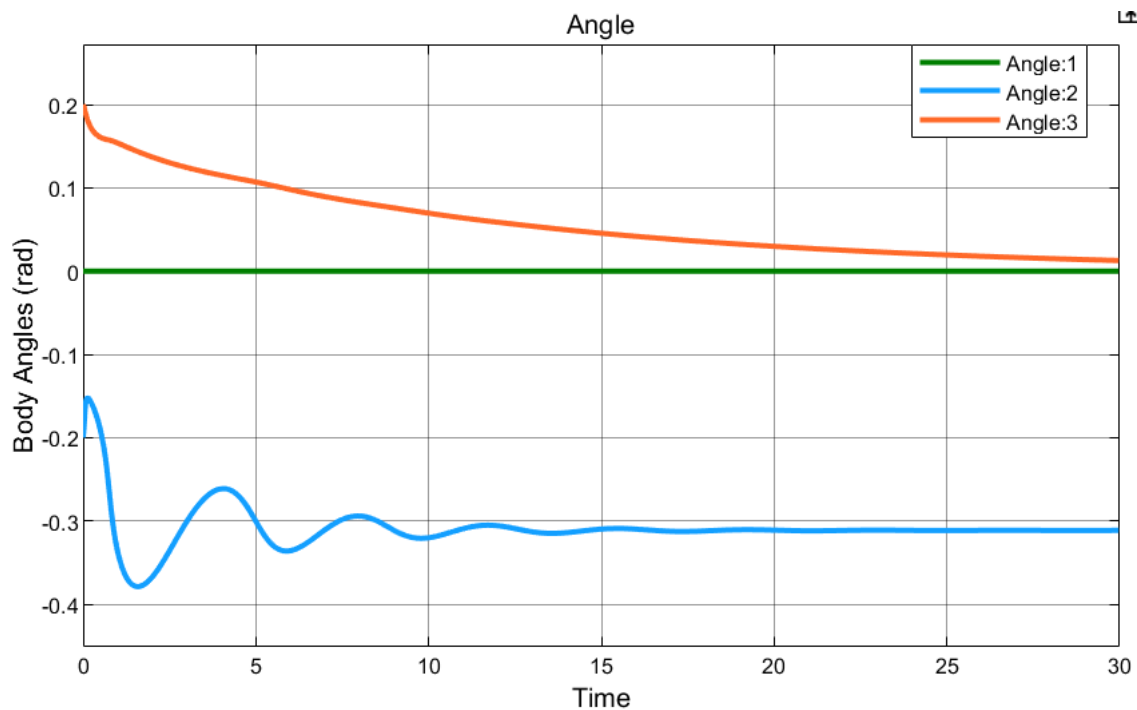


Figure 29: Alpha body angles control off

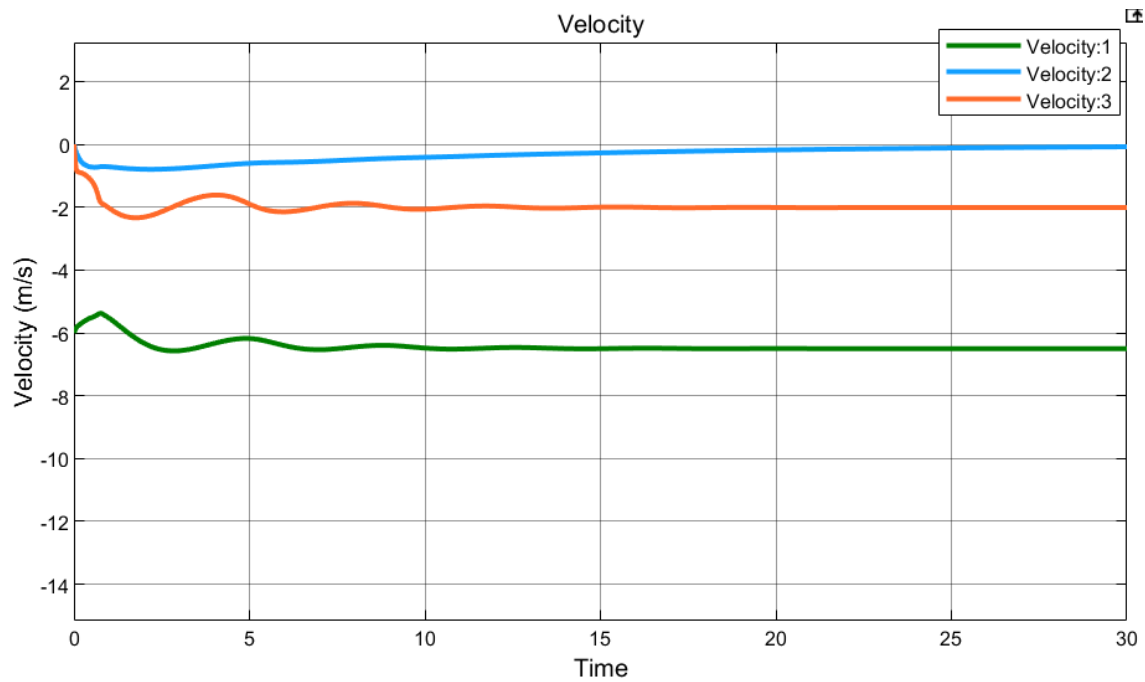


Figure 30: Alpha velocity control off

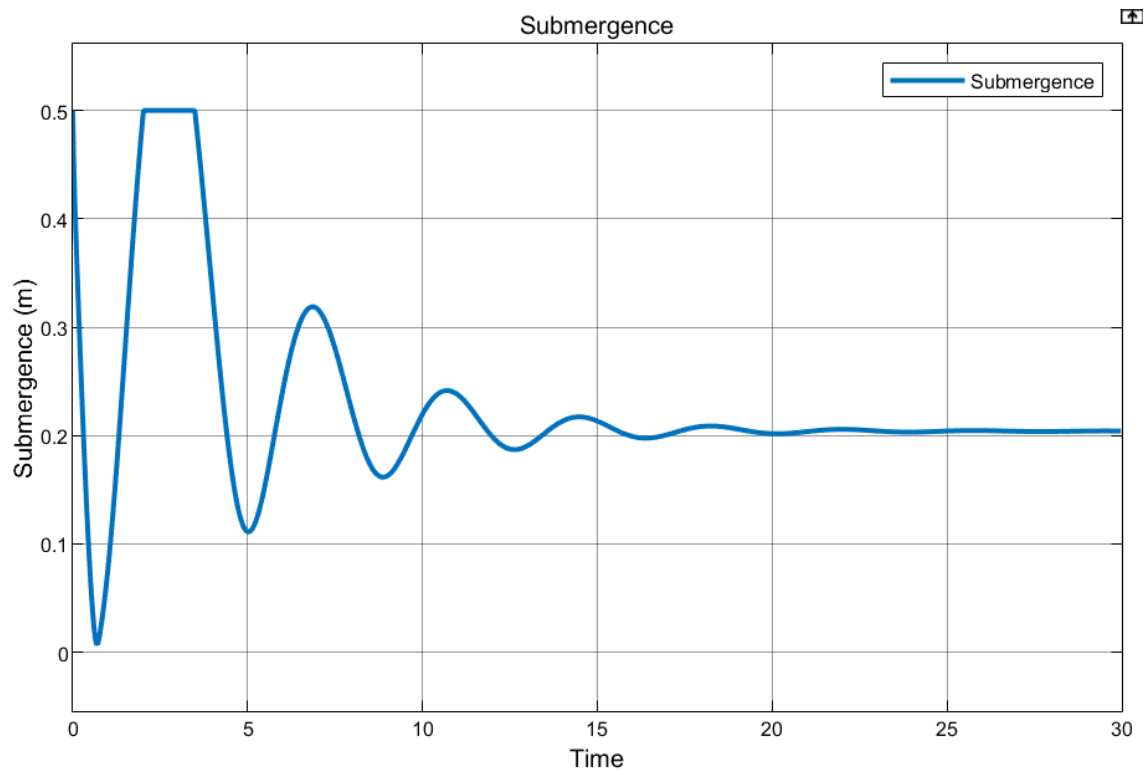


Figure 31: Alpha submergence control off

And next, the results of the platform with the control turned on, so, the rider tries to minimize the oscillations:

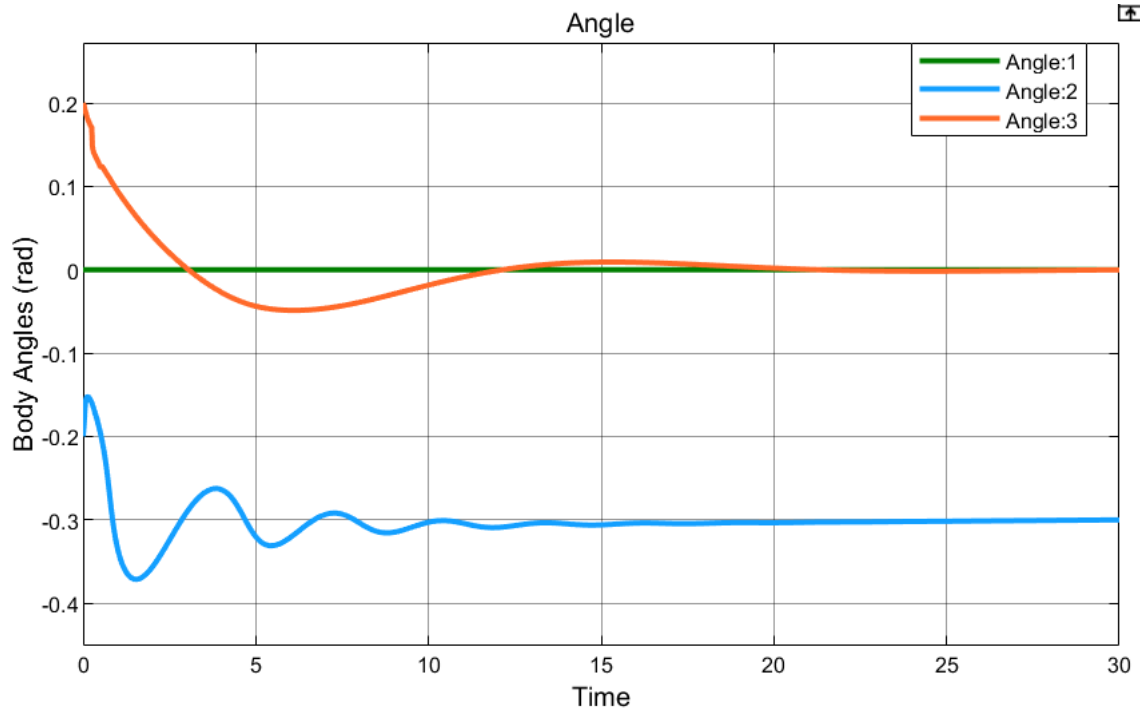


Figure 32: Alpha body angles control on

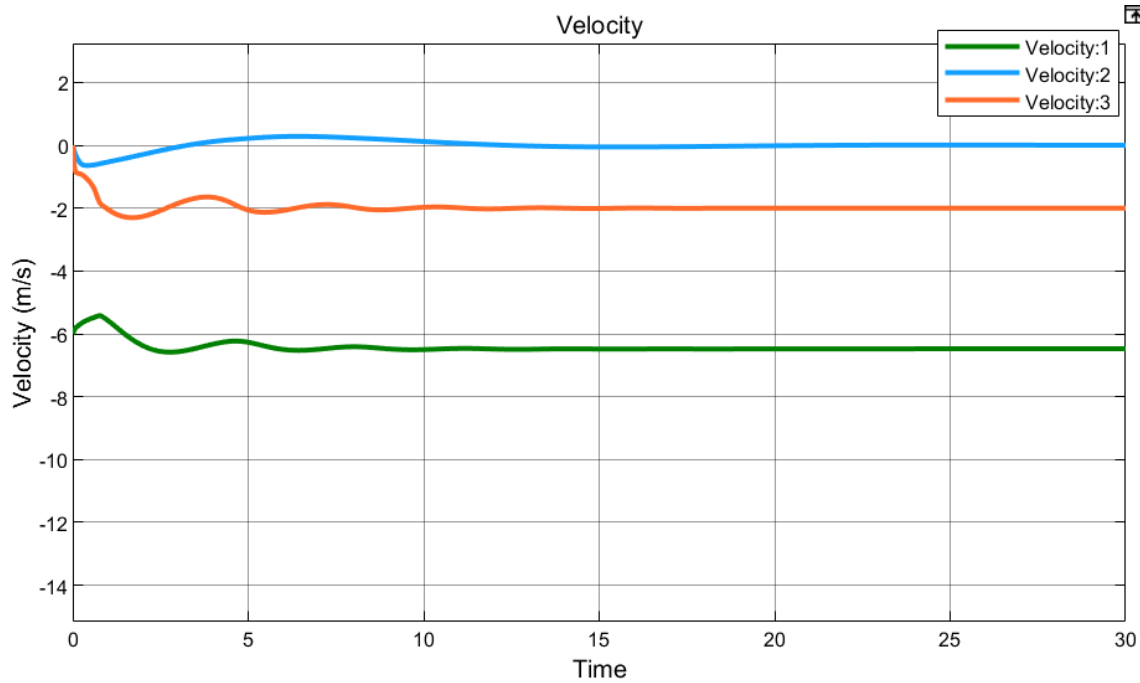


Figure 33: Alpha Velocity control on

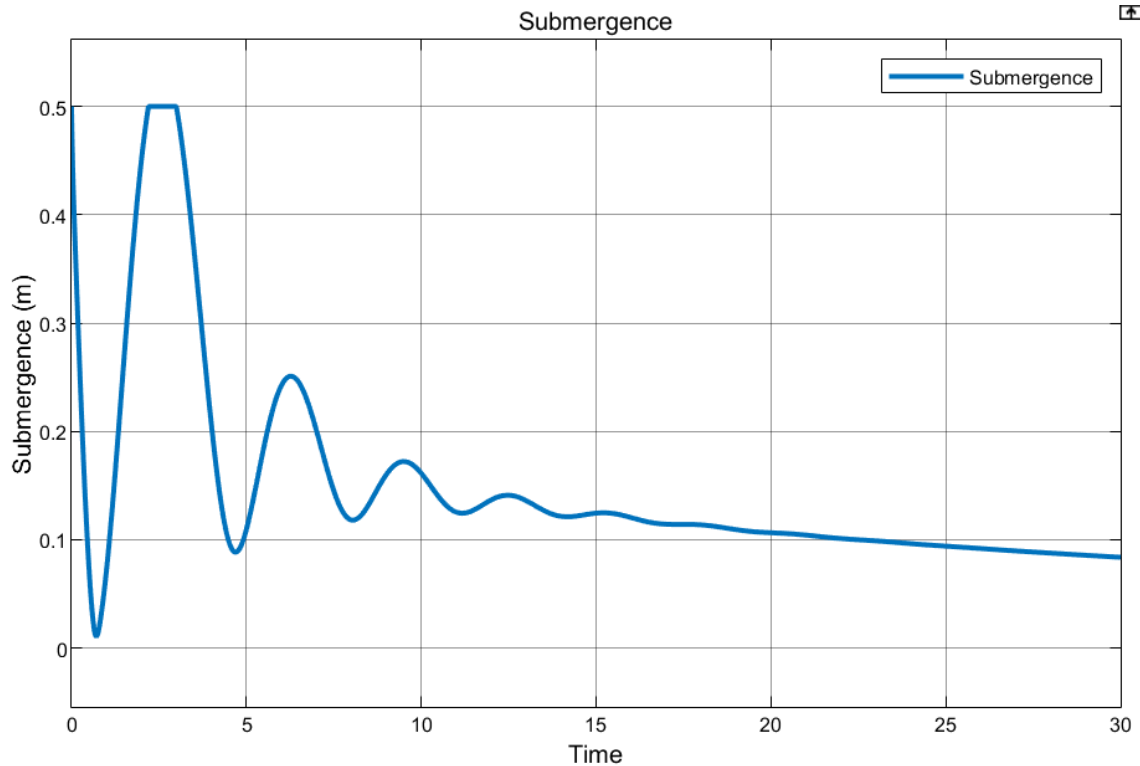


Figure 34: Alpha submergence control on

3.5.2 Beta

Beta needed at least $\delta = 19^\circ$ of wave inclination to reach the take-off speed. The following results are with the control turned off:

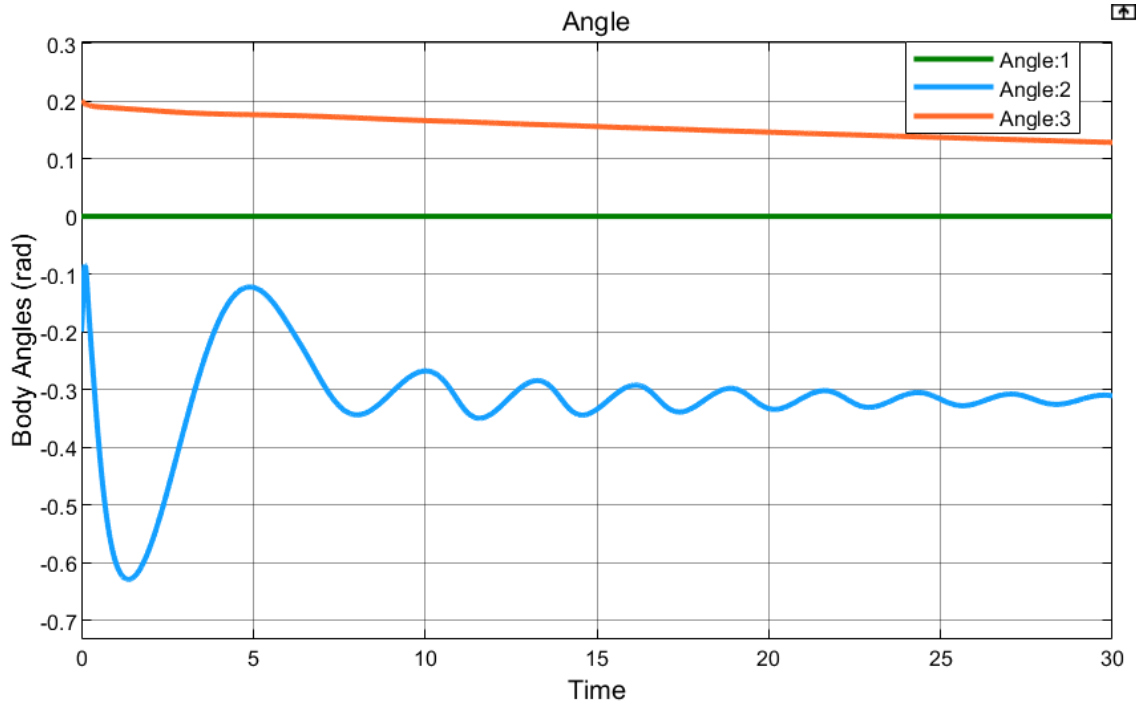


Figure 35: Beta body angles control off

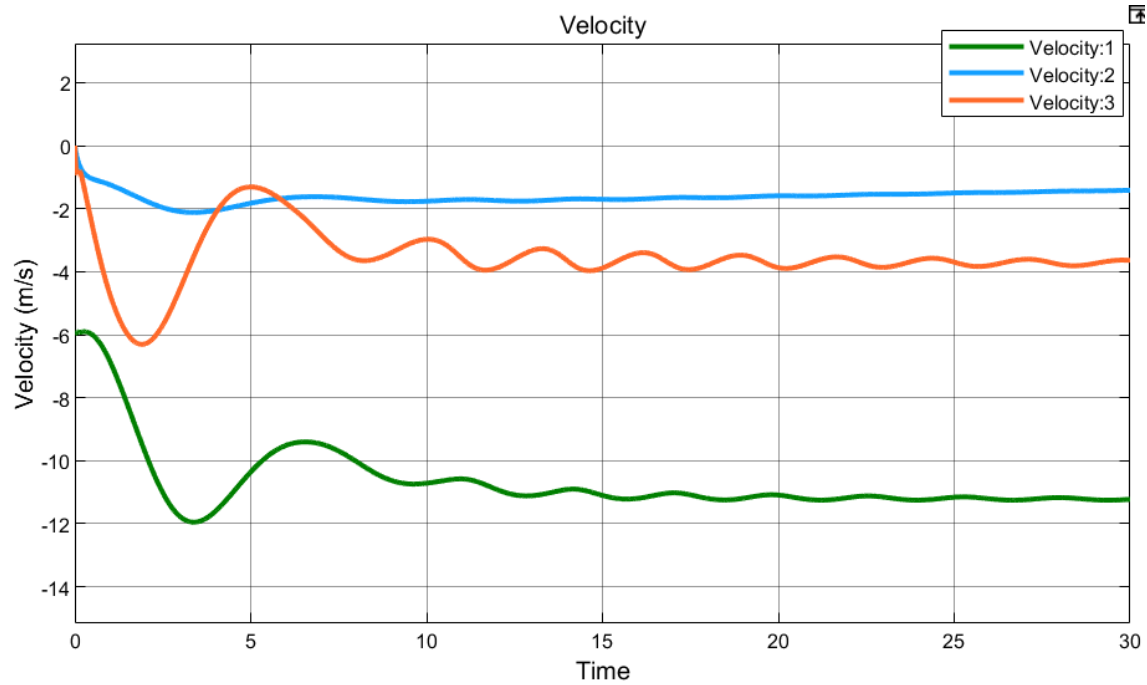


Figure 36: Beta velocity control off

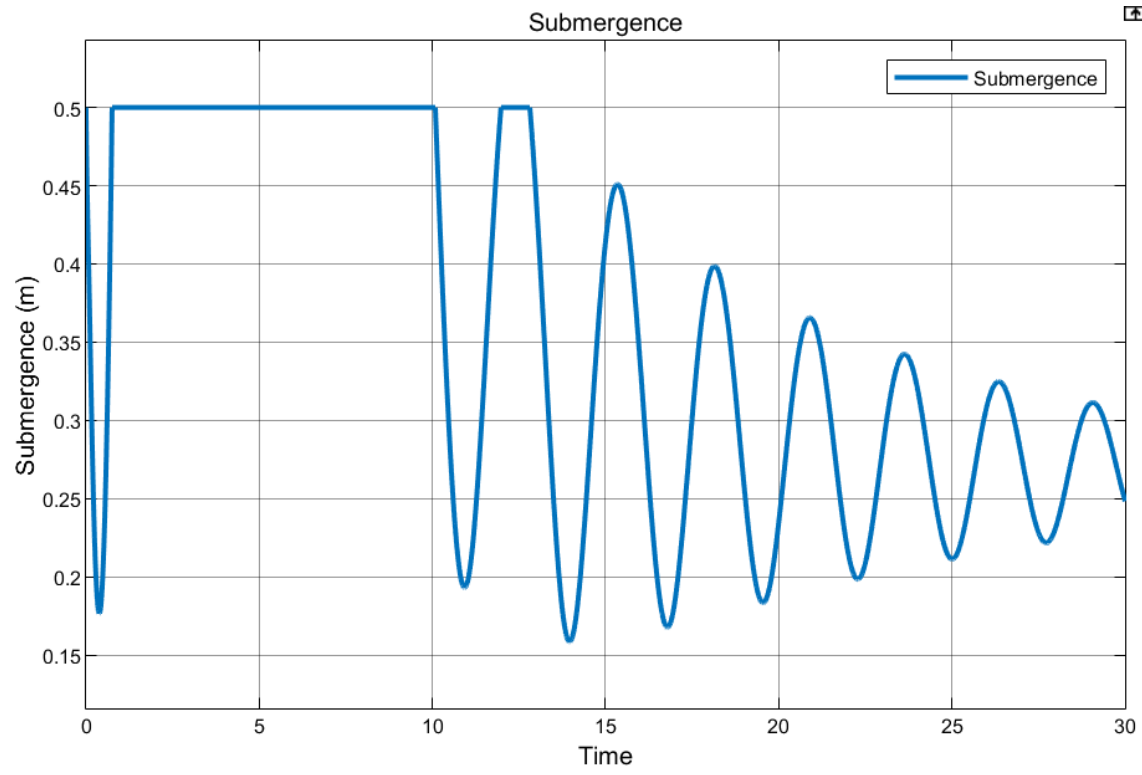


Figure 37: Beta submersion control off

The next graphs show the results of Beta with the control turned on:

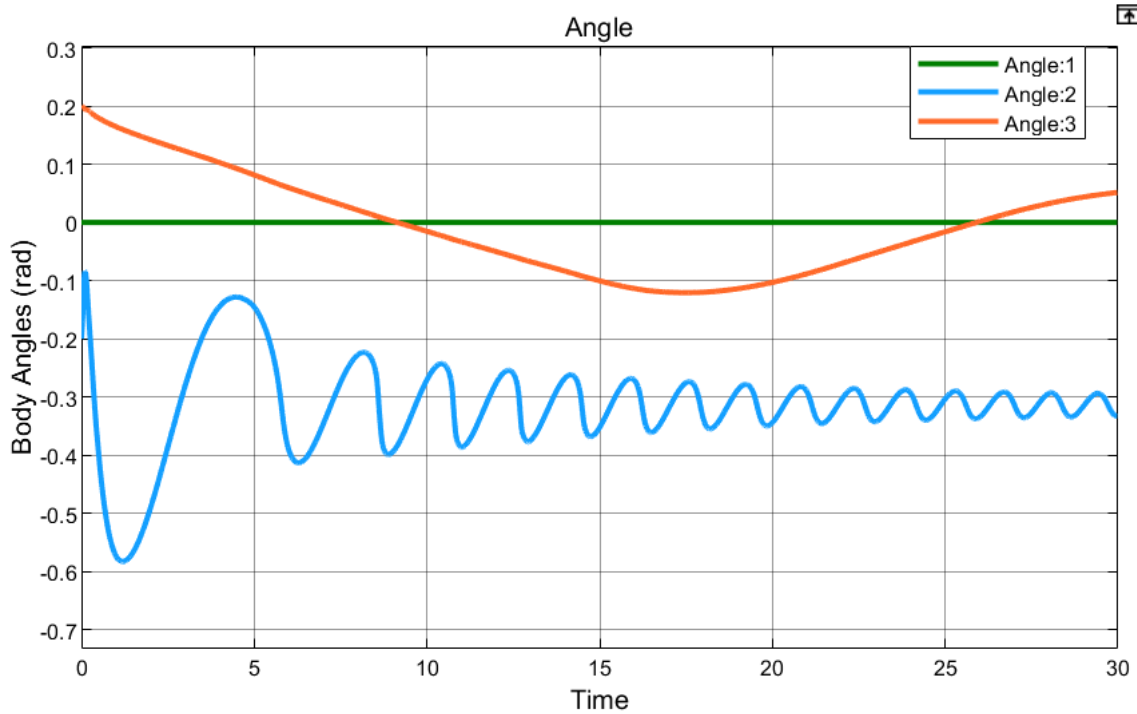


Figure 38: Beta body angles control on

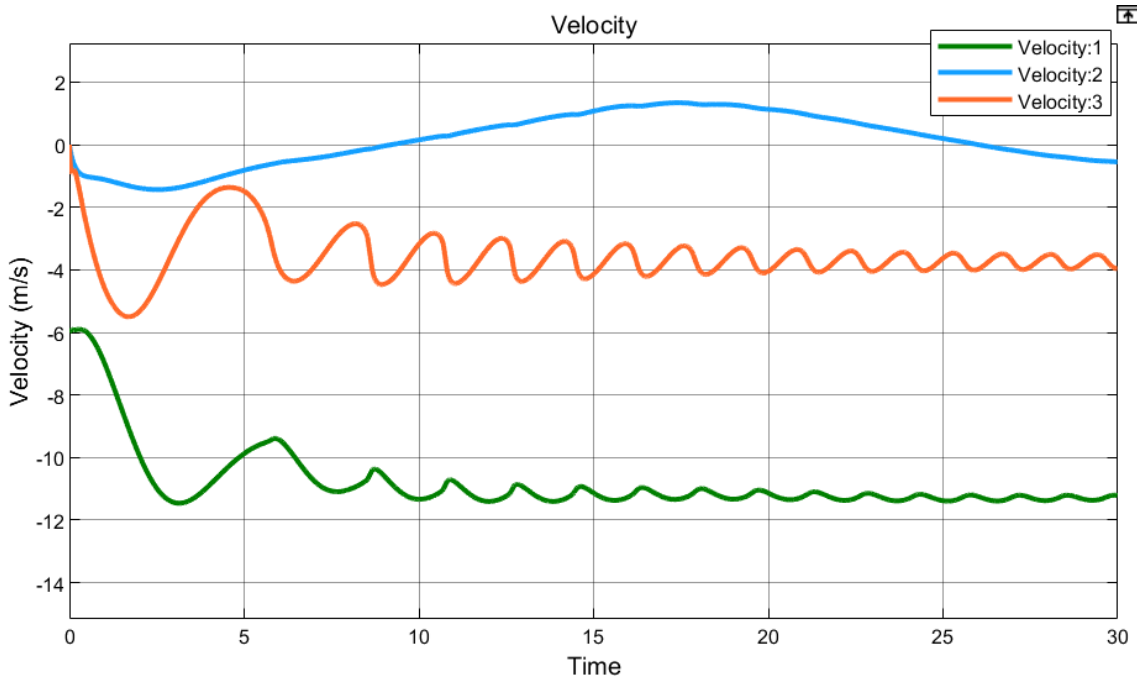


Figure 39: Beta velocity control on

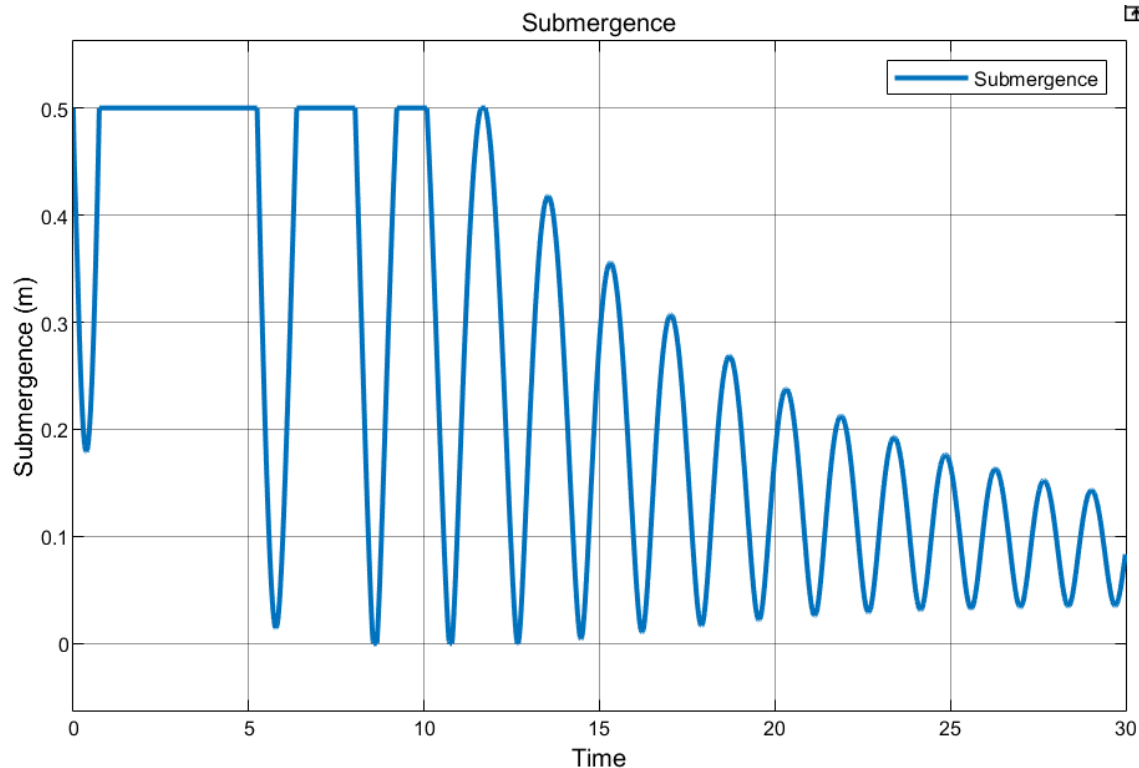


Figure 40: Beta submergence control on

3.5.3 Comparison

From Alpha, it can be seen in Figure 29 and in Figure 32 that over angle 2, which is θ , the control does not have an appreciable effect. However, the angle 3, which is ψ , needs the control to dissipate the oscillation. In both Figure 30 and Figure 33 can be seen that the velocity needed to maintain the flight is 6.5m/s. It can be seen in Figure 31 and Figure 34 that when the control is turned on the height of the board becomes steady faster than when it is turned off. Also, the submergence of the foil without control is higher.

From Beta, it can be observed the same phenomenon reported in Alpha, the control is needed for stabilizing the angle ψ , as it can be seen in Figure 35 and Figure 38. However, in these figures and also in Figure 37 and Figure 40, when the control is turned on it becomes more oscillating. Finally, in both Figure 36 and Figure 39 the speed needed to maintain the flight is 11m/s.

These results show that Beta should have worst behaviour than Alpha, is more oscillating, it does not benefit from the active control and its take-off speed is almost twice the value of Alpha's. For this reason, the wave needed for Beta is also almost twice as sloped. Considering that low wave conditions was an objective, is clear that Alpha should be better option. However, both geometries will be constructed at scale and tested. After the tests, a decision making will choose the final geometry to build at real scale.

4. Model

The objective of this part is to build at 1:5 scale model that is able to accept different plane configurations printed with a 3D printer. The centre of mass position needs to be variable at will.

The tests developed in this section will be used to decide the final geometry, but they can also be compared with the Simulink platform results. If those results coincide, in the future, the Simulink platform could be used to assess the dynamic stability without needing the scale tests.

4.1 Construction

In the following pages, the construction of this model will be explained part by part. The following figure is an image of the whole model in a test.



Figure 41: Scale model test

4.1.1 Geometry

The first step was to export the Open VSP geometry to a Cad software, in this case, Autodesk Fusion 360. This software has a student license which is open source. The Open VSP geometry was exported as an STL, which describes the geometry with triangles. Also, the analysis geometry has a shorter vertical stabilizer because not all of it is inside the water when the hydrofoil is lifting. This was then imported into Fusion 360 which converts the hole shape into a body. The wing, the tail and the fuselage had to be combined because they were interpreted as separated bodies. Then, a perpendicular support plate to the vertical stabilizer was designed with 4 holes for M3 screws. The model needed to be scaled to the correct size, 1:5. This is the maximum scale that fits on the 3D printer. Before printing, the whole model was cut by its X-Z symmetry plane. This made it possible to print the wing and tail in the best orientation for avoiding layer manufacture inaccuracy and also avoids the use of support material. The central fuselage was also enlarged in order to resist the bending loads.

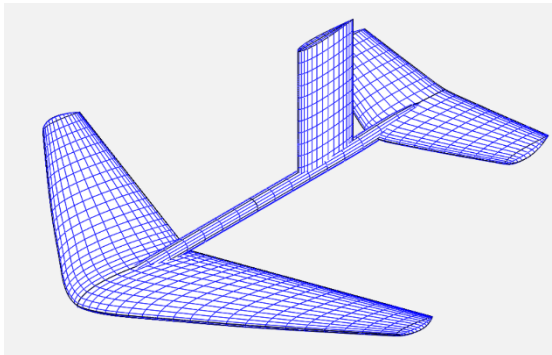


Figure 42: Open VSP geometry



Figure 43: Ready to print geometry

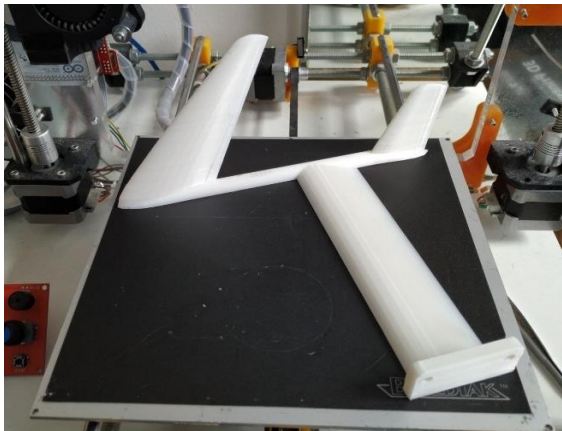


Figure 44: 3d printed Alpha geometry

From Fusion 360 the model is exported in STL to the slicer program Simplify3D.

The printing settings were 100% infill density in order to obtain a solid piece of plastic which is more resistant and also has no risk in water problems. The layer height was set to 0.25mm with 3 outside perimeters. The nozzle temperature was 235 °C and the heated bed was set to 60°C. The plastic used was PLA from Sunlu brand. Each half took 5h to print and 82g of plastic were used.

After the 2 halves were printed, the inner flat surface was sanded, preparing it to be glued with epoxy glue of *Supertite* brand. This glue is optimal for this job because it is water resistant and sticks very well the plastic used to print. After assembling the two parts together, the excess glue of the joint was sanded to obtain a smooth transition between halves.

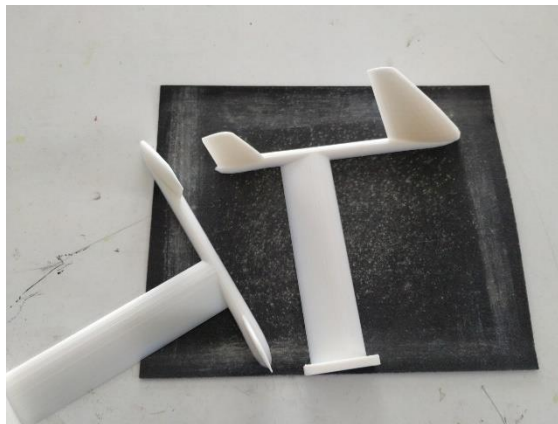


Figure 45: Surface treatment for gluing



Figure 46: Gluing process

This explanation was for the Alpha configuration. However, Beta was done exactly like described before but adding a plastic arm to place the wing in the desired position. In addition, for Beta design was not possible to avoid support material because the winglet that acts like a vertical stabilizer was perpendicular to the wing. Each half took 7h to print and 115g of plastic were used.



Figure 47: 3d printed Beta geometry

Next, a photo of the final result for each design is presented.



Figure 48: Final Alpha geometry



Figure 49: Final Beta geometry

4.1.2 Surf Board

A wood surf board have been constructed to contribute floatability and central attachment for all the components. The explanation of its construction will be found in the Annex section.

4.1.3 Sliding Mass

The objective of the sliding mass is to control the centre of mass position at will.

The design chosen is a 3d printer like motor with a pulley on its axis and a static belt. The battery was mounted over the motor and the whole weight can slide on two rails and can precisely control its position. The first idea was to implement an accelerometer and a PID to active stabilize the model but this idea was declined as it will be explained later on. Instead of the accelerometer, the position was finally controlled by radio control receiver. Furthermore, all the electronics need to be in a waterproof box.

The first step was to design everything in fusion 360. One major problem was the need to put everything inside a hermetic box. So, there is no space for oversizing the parts. In fact, the first idea was to build an acrylic box and all the dimensions were adjusted to 100mm wide but when all the pieces were printed and was successfully working a better solution was found; which was an acrylic food case found on the local store. Unluckily, the maximum wide accepted by this case was 80mm. Also, the height was limited to 90mm. However, the food case was overall better option because of its industrial manufacture which ensures hermeticity. So, a redesign and reprint of the pieces was done. There are 8 3d printed pieces in this construction. All of them were printed with the same settings as the wings, 100% infill and pla plastic. The new wood base was CNC cut. The next image shows all the components bought for the construction of the sliding mass.

- A nema 17hs4401 stepper motor with its A4988 stepper driver
- 1m of gt2 open belt
- A 32 teeth gt2 pulley
- An Arduino Uno
- A 3 cells Lithium Polymer battery with 1.3 Ah of capacity
- The accelerometer MPU6050 and the radio transmitter Turnigy 6ch are not in this figure because it was not necessary to buy them.



Figure 50: Components of the sliding mass system

The central piece is the one that holds the motor. It also holds the two 608 bearings. These are used to guide the belt through the pulley attached to the motor axis. This is because the motor is mobile and the belt is static. This central piece also acts as the linear bearings for the 8mm aluminium tubs that act as linear guides. This was possible by making the hole slightly bigger than the tube diameter, 8.2mm, together with some grease to reduce the friction. This piece required support material and took 4h to print. A few images are now attached to show this mechanism.



Figure 52: Central piece printed



Figure 51: Central piece assembled

There are 4 pieces that act as a tub holder to join the two aluminium tubs to the piece of wood. There are 2 more plastic pieces which fix the belt to the wood. The last piece is a battery and Arduino holder which is mounted over the motor. These other pieces took 3h to print.

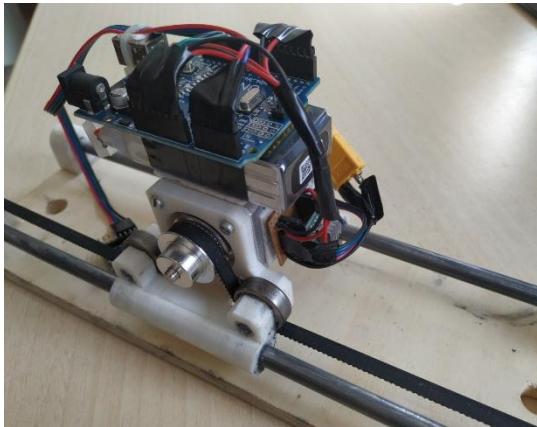


Figure 54: The first design approach

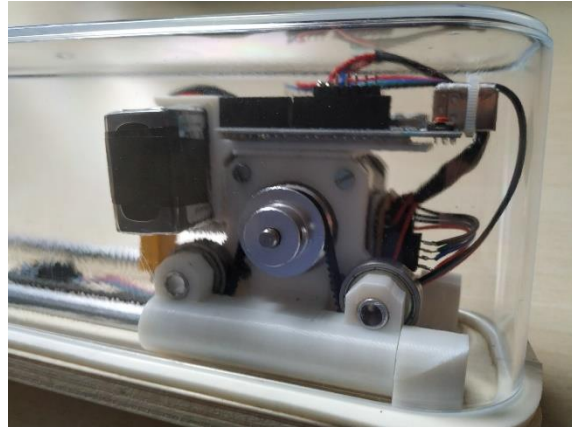


Figure 53: The final design

The next point is the electric circuit. The brain of this circuit is the Arduino Uno. The Arduino Uno can be programmed using the Arduino IDE, an open source software based on C++. The microcontroller is powered by the 12v LiPo battery. It has a dc to dc converter which can reduce the voltage to 3.3 and 5V. These voltages are suitable for powering the other devices: the accelerometer, the radio receiver and the logic part of the stepper driver. The Arduino receives information from the accelerometer or the radio controller, it processes the inputs and elaborates a suitable output which goes to the stepper motor driver. The driver transforms the serial data into the input for the motor which is the high-power part of the whole electric circuit and it is powered directly from the battery. Then, the motor spins precisely and maintains its position until the next move.

A connections photo is attached but with the Arduino Nano instead of the Uno as will be later explained. As it can be seen, the Arduino Nano and the stepper motor driver needed a pcb to be connected. These pcbs were made out of a virgin breadboard and the inner connections were done using tin channels.

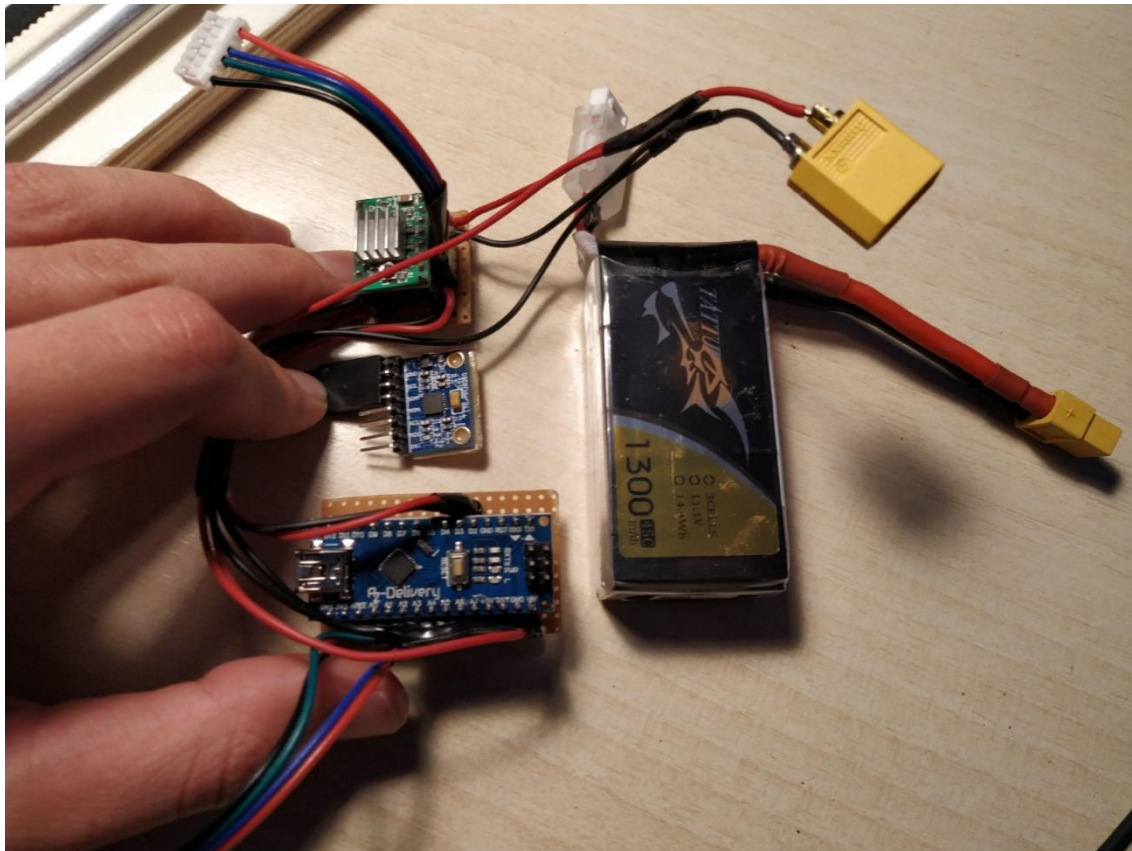


Figure 56: Connections photo

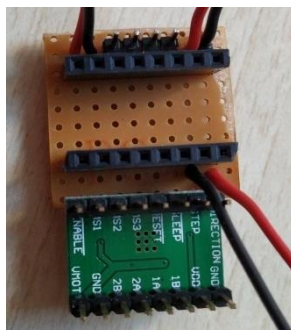


Figure 57: Custom driver pcb

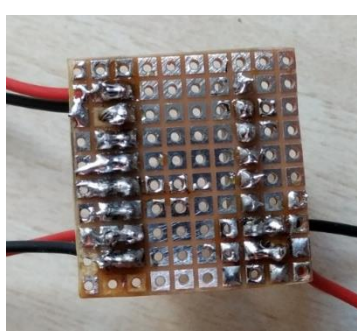


Figure 58: Tin channels

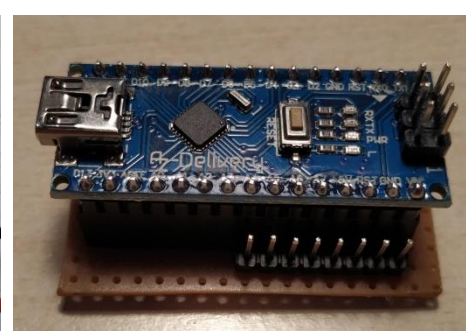


Figure 55: Custom Arduino NANO pcb

As it can be seen in Figure 54, which was the first design before the food case, the height was not a problem and the Arduino was mounted over the battery and the battery over the motor. However, the food case introduced height limitation and the Arduino Uno was not an option so an Arduino Nano was bought. The Nano has almost the same features than the Uno in a much smaller form factor. The C++ code is the same for both. The code uses interrupts to send information to the motor driver and once every 10ms the accelerometer is read and the desired position changes with the angle of the accelerometer. If the surf board pitch down the mass move backwards and it moves to the front if the surf pitch up.

The design of the Figure 54 was fully functional and had no problems. Then, the dimensions reduction made the Arduino Nano better option than the Uno. But there was a problem with the Arduino Nano. After elaborating the pcb and reconnecting all the cables; the same code uploaded to the Uno did not work properly on the Nano. The mass slide properly during a few seconds but after that it always moved to one end of the rail and crashed. After revising all the connections, the problem was not resolved. Suddenly after a few tries, the accelerometer blew up. After buying another accelerometer and installing it again, the randomly crashes did not resolve. Then, the Arduino Uno which has worked well was connected again. Unluckily, the connections were wrong and the microcontroller blew up because of a short circuit. After buying another Arduino Uno and soldering all the connections again, the same problem of the Arduino Nano started to occur. The system just worked during about 20 seconds. It was not a code problem because disconnecting the motor and observing the plot signal of the Arduino IDE there were no cracks or suddenly stops, everything was smooth and running right during more than 1 hour. After an online search, it was found in (Arduino Forum, 2019) this problem can come from irregularities in input voltage produced by the a4988 driver and the solution found was to connect a ceramic capacitor of 100nF in parallel with the 5 or 3.3V and the ground. This method blew up the accelerometer again and it was at this point where the idea of active stability controlled by the accelerometer was discarded. Next, an image of all the components bought that ended burnt or without use:

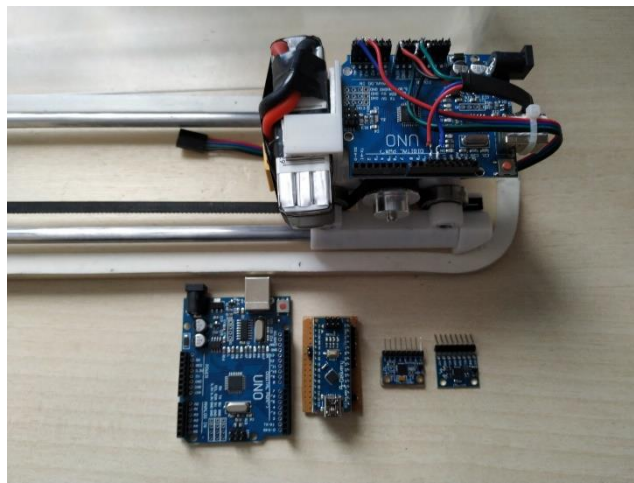


Figure 59: Failed electronic components

The final solution was to connect a radio-controlled receiver which can be read by the Arduino and transform the signal to be proportional to the position of the mass. In this manner, the stick position of the transmitter controls the position of the centre of mass of the surf board. Next, a photo of the final sliding mass system.

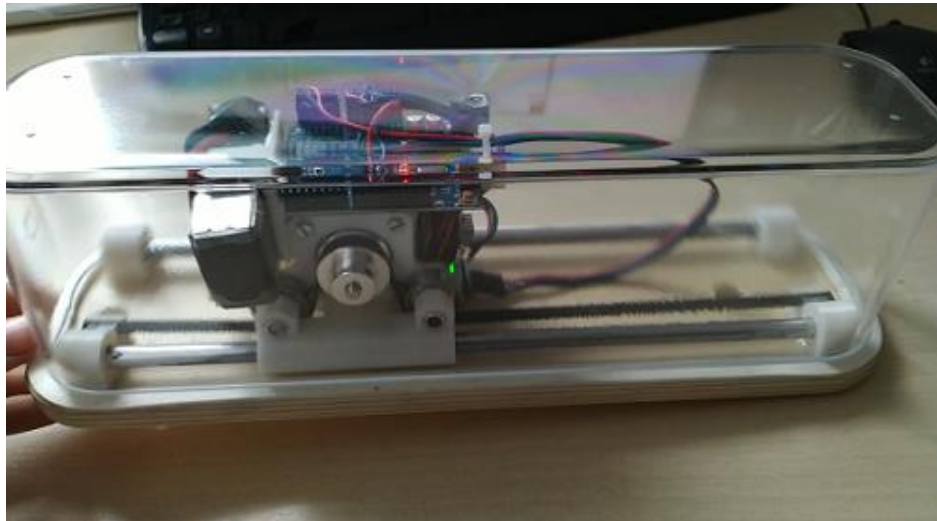


Figure 60: Final sliding mass system

Finally, to ensure a proper water resistance, a plastic like window seal was glued to the perimeter of the wood piece in the location where the food case made contact. Some plastic flanges ensure a strong union between the acrylic case and the wood. Two 300mm aluminium tubs with a diameter of 12mm were located between the surf board and the sliding mass in order to have the centre of mass located at 300mm above the wing tip, just one fifth of the distance between the wing tip and the centre of mass of the real model.

At this point, the model was ready for the tests. A test bench was needed to develop the test and will be explained in the next section. A few images of the final model constructed are attached.



Figure 61: Final scale model constructed



Figure 63: Render of the model

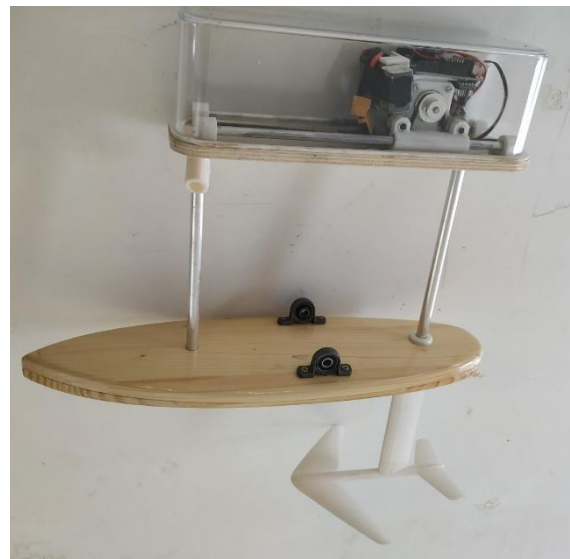


Figure 62: Real model for comparison

Characteristics	Value
Mass	1910g
Floatability	15N
Centre of mass displacement	46mm
Speed range	0-3m/s

Table 7: Model characteristics

4.1.4 Articulated quadrilateral

The bench test function is to create a controlled environment where the desired characteristics can be studied. In this case was very important to restrict some degrees of freedom because there are six in total. However, only two of them have been studied, the vertical position and the pitching angle.

In order to restrict the other 4 degrees of freedom an articulated quadrilateral has been developed. This quadrilateral needs to have a tub at the end where two bearings are located and attached to the surf board. In this way, the quadrilateral allows vertical movement and the bearings allow pitching freedom. This idea was inspired by the trapezoidal suspension of a car and its wheel bearing. Some images are now attached for the better understanding of the system:



Figure 65: Articulated quadrilateral build

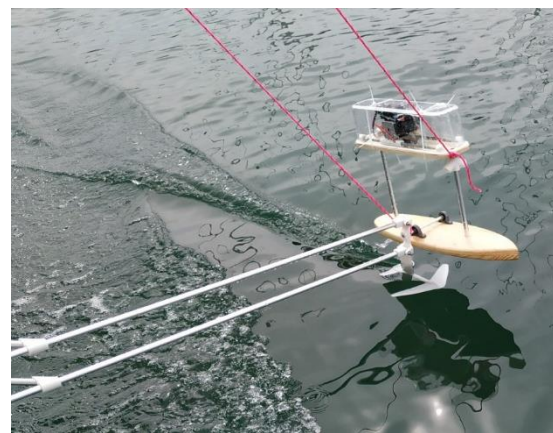


Figure 64: Articulated quadrilateral on a test

The big piece of white wood where the quadrilateral is attached is collocated on the boarding of a boat which can vary its speed. So, at the end, the speed of the board can be controlled, it cannot move sideways, the roll and yaw rotations are restricted and the only free movements are the vertical position and the pitching angle.

In order to control the pitching moment and the vertical position, two ropes were fixed to the surfboard. One of them was located at the tip tub of the quadrilateral so it only affects the vertical position. The other was fixed at the front aluminium tub and allowed to rotate the model at will. These ropes can be seen in Figure 64.

The construction of the articulated quadrilateral consisted in 4 aluminium tubs, two of them were 1m long and the other two were 30cm long; all of them were 12mm in diameter. The short ones were located at the root and form a 45° angle. Their propose was to avoid bending



Figure 67: Plastic tub ends joints



Figure 67: Aluminium hinge inserts

moments on the root joints. All the white pieces that can be seen on the Figure 65 were 3D printed. There was a total of eleven printed parts which took 12 hours to print. Six of them were tub ends with a 6mm hole. Short aluminium tubs were located in those holes to act as a hinge in conjunction with M4 inox screws.

There were two more pieces which act as the other half of the hinge between the white wood and tub ends. In these parts was where the screws were tightened. The bearing axel was also joint with a plastic piece as it is shown in the next image:



Figure 69: Quadrilateral root



Figure 68: Quadrilateral tip

Finally, two kp008 bearings were attached to the surfboard. The position of them was modified after the first test, as it would be explained on the next section.



Figure 71: First bearings position



Figure 70: Definitive bearings position

4.2 Tests

All the tests developed in this study were qualitative. In these tests, there were 3 aspects to evaluate.

- Stability: is the most important aspect. To evaluate it, only the central rope was pulled. This means that the whole model was free to pitch. In this situation, the surf board needed to be able to maintain an angle. If it did, the other rope (the one that can change the angle) could be pulled to simulate perturbations. The board needed to dissipate the perturbations and return to its equilibrium position.
- Lift at its equilibrium point: this aspect was studied by knowing how much force was required in the central rope to maintain the vertical position constant. If a lot of force was needed, the hydrofoil was lifting poorly but if the force required was lower or even zero, the hydrodynamic forces were compensating the weight.
- Centre of mass position: In this test, the sliding mass is positioned most delayed position possible. The more delayed the centre of mass, the higher the angle of attack and greater the lift but it becomes more unstable till the point where is not possible to maintain the equilibrated position.

Four tests have been done to evaluate the geometries.

4.2.1 First test

The first test was on 11th of April and only the geometry Alpha was been printed for this day. In this test day, the bearings were located in the centre of mass height. This did not produce any torque in the centre of mass reference but does not represent the mechanics of surfing. The force that moves forward the surf board is the component of lift projected forward, like a sailing plane, which is applied in the aerodynamic centre. Pulling the board from the centre of mass caused the drag force, multiplied by the 30cm distance in between, to produce a moment that made the board pitch down. This effect was incremented the faster the test was done. This leaded to a major problem which was that there was or not enough speed or not enough angle of attack and the hydrofoil was not able to sustain itself.

To make the board pitch up the centre of mass can be delayed but this also destabilize the model. With the sliding mass almost at the most delayed position, the foil was able to maintain an equilibrated angle with only a slight tension on the central rope. However, the smallest perturbation introduced was not able to be dissipated.

4.2.2 Second test

To solve the problem encountered the first test day, the pull position was lowered on the base of the surfboard as it can be seen in Figure 70. Ideally, the pulling position should be the aerodynamic centre where the lift is produced and therefore the pulling force. However, the tip tub of the articulated quadrilateral would have a major effect on the fluid, so, the lowest possible position was just over the water. These leads in a noticeable improvement of the tests.

In this second test day, Alpha was also the only geometry available. The new pulling position made possible that the foil had a much better performance and, in addition with the not so delayed centre of mass, the model was way more stable and less force was needed in the central rope; even reaching zero force as it can be seen in the following image. The two ropes are hanging and not transmitting any force to the model:



Figure 72: Second test. No tension on the ropes

This was a successful test and established a reference to compare with the other geometry. The tension in the rope, the level of perturbation dissipation and the optimum and most delayed position of the sliding mass.

4.2.3 Third test

For this test day the geometry Beta was already printed and prepared to be used. Even though, the first part of the test was done with Alpha to corroborate the results obtained in the second test.

After developing the test, the geometry Beta did not obtain the same results as Alpha. The equilibrium angle was possible but the lift produced at this position was small and a lot of force on the central rope was needed. In addition, the perturbations were fast amplified and the equilibrium was lost in a few seconds. Moreover, the mass needed to be past the half line, any more delayed position was not able to be equilibrated. It also was very sensible to mass moves.

4.2.4 Fourth test

This test was a replica of the third session, the two different geometries were put to the test. However, Aleix Báez, the director of this degree final project was able to assist and help with the development of the test. The results obtained where very similar in comparison with the third session, overall, the geometry Alpha had a better performance than Beta. Nevertheless, to take the adequate geometry an OWA decision making needs to be done because there are other factors which affect the decision.

4.3 Decision making

In order to take the appropriated decision an ordered weighted averaged method will be used, an OWA. To use this methodology, all the parameters need to be explained and weighted before. All the parameters will have a punctuation from 0, meaning very poor behaviour, to 5 which is perfect performance. Next, a list of the parameters considered.

- Stability: it represents the ability of dissipating the perturbations induced and remaining on the equilibrated angle. It has a weight of 5.
- Lift: it represents the sustentation force made by the foil at its equilibrated position. It has a weight of 3.
- CoM: centre of mass, it represents the range of possible positions of the CoM where the board remains equilibrated. It has a weight of 2.
- Molds: the number and difficulty of the molds that need to be manufactured with the CNC machine in order to create the outer shape of the real scale geometry. It has a weight of 4.
- Structure: The internal stainless-steel structure needed to withstand the loads. It has a weight of 3.
- Cost: The material cost. It has a weight of 2.
- Aesthetics: how much beautiful it looks, it is a subjective aspect. It has a weight of 1.

OWA	Alpha		Beta		
Criteria	P	PxWeight	P	PxWeight	Weight
Stability	4	20	2	10	5
Lift	4	12	2	6	3
CoM	3	6	2	4	2
Molds	3	12	2	8	4
Structure	1	3	4	12	3
Cost	3	6	3	6	2
Aesthetics	2	2	4	4	1
Sum of PxWeight	-	61	-	50	
Max of PxWeight		100			
OWA	0.61		0.5		

Table 8: OWA decision making

The OWA shows Alpha as the geometry to choose and therefore it will be the one to build in real scale.

5. Real Scale Model

In this section the construction and testing of the real scale model of the geometry Alpha will be explained.

5.1 Structural design

The structural design will be separated in two parts, the internal stain-less structure and the composite material lifting surfaces.

5.1.1 Internal structure

The internal structure is the responsible of withstand the loads produced by the wing and tail and transport them into the board where the rider stands on. Next, a photo of the final model on fusion 360:



Figure 73: Final internal structure render

Stainless steel has been the choice to build the internal structure because its oxidation resistance, its strength and its ability to be soldered and accomplish strong joints. From the design, the distance between the leading edge of the wing and tail is 1m. So, the central tub will have the same length. In order to size the tub, the maximum load factor that will be assumed is n=4. This means that if the total weight is 800N, during a n=4 maneuver the lift produced is 3200N. It can be assumed that the wing is doing all the lift, to be more conservative. Since the tail has 3 times less surface than the wing, it can also be assumed that the maximum lift produced by the tail it is one third of the produced by the wing, 1067N.

It was at this point when it was clear that a change in the design was needed. In the first approach of geometry Alpha, there was not vertical stabilizer because the vertical support acted as it. To do so, the vertical support needed to be delayed leaving a large distance between it and the wing; the principal font of hydrodynamic forces. In the first approach, the vertical stabilizer was located at 0.6m of the wing. This would produce a large torque as it can be seen in the next image:

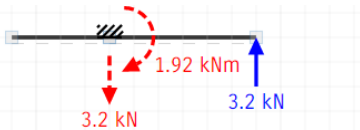


Figure 74: First central tub wing load diagram

The central tub needed to withstand 1920Nm. This is a very high torque and would need a large inertia which would be excessive for resisting the tail loads. The next image describes the situation:

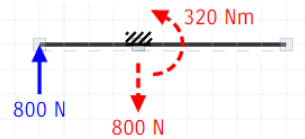


Figure 75: First central tub tail load diagram

In the tail case, the tub would need to resist a moment 6 times smaller. To solve this problem, the vertical support can be located at 0.25m from the front end and, because the central tub is 1 m long, at 0.75m from the back end. This leads in the same torque produced by the wing and tail at maximum lift condition as it can be shown in the following images.

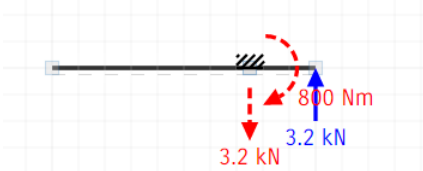


Figure 76: Final central tub wing load diagram

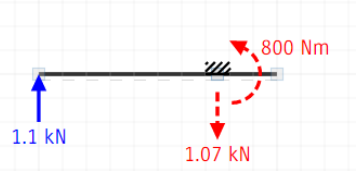


Figure 77: Final central tub tail load diagram

This means that using the structures equation: $\sigma = \frac{M}{I} \cdot y$ (Wikipedia Bending, 2019), the maximum stress which is able to resist the stainless steel: 550 MPa (Azo Materials, 2019) and the inertia of a circular hollow tub: $I = \frac{\pi}{4} \cdot (r_{out}^4 - r_{in}^4)$ (Wikipedia Second Moments of Inertia, 2019) the 30mm tub with 3mm wall give these results:

$$I = \frac{\pi}{4} \cdot (r_{out}^4 - r_{in}^4) = \frac{\pi}{4} \cdot (15mm^4 - 12mm^4) = 2.35 \cdot 10^4 mm^4$$

$$\sigma = \frac{M}{I} \cdot y = \frac{8 \cdot 10^5 Nmm}{2.35 \cdot 10^4 mm^4} \cdot 15mm = 510 MPa$$

$$\eta = \frac{\sigma_{max}}{\sigma} = \frac{550}{510} = 1.08$$

Once the central tub was chosen, the vertical support tub will be the same because it implicates a cost reduction. Both the central and the vertical tub are chosen to be circular in order to reduce drag.

5.1.2 Lifting surfaces

The lifting surfaces will be constructed in composite materials. More precisely, in chopped glass fibre of 300g/m² with unsaturated polyester resin as matrix.

The structure chosen to build the real scale model is monocoque. To avoid buckling of the fibre parts polyurethane expansion foam will be added as a solid core. This technique will also prevent water to enter inside. Since the foam expands and adopts any shape, the minor manufacture problems such as irregular skin thickness will self-address. It will be used in the tail, in the vertical stabilizer and also in the wing. In addition, in all of them there will be a central stainless-steel beam which will also take part of the loads. However, for this study only the fibre resistance will be considered.

As will be later explained in the section 5.2.3 Lifting surfaces, a first trial was done to know the fibre to resin ratio and the thickness of the composite as function of the number of layers. These values are 60% in weight and 0.375mm per layer respectively.

To be more conservative, a constant distributed load will be considered in this study. In the next image, only half of the wing is showed in the load diagram. The wing distributed load is 3200N/m at n=4 since the span is 1m and the load 3200N. The same applies for the tail but since its span is 0.5m and the load at n=4 is 1067N, the distributed load is 2134N/m.

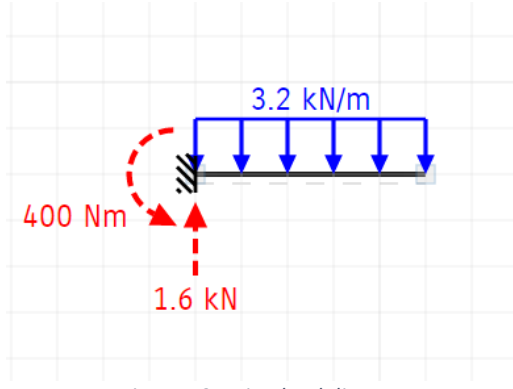


Figure 79: Wing load diagram

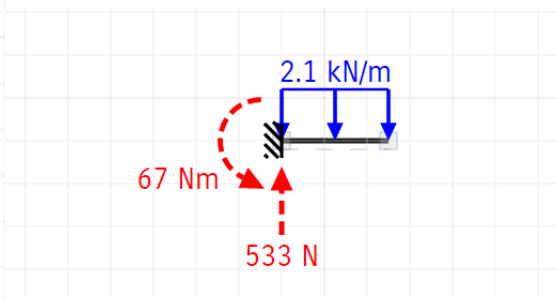


Figure 78: Tail load diagram

For the wing, it can be seen that the total moment applied at the root is 400Nm. The maximum tensile strength of the glass fibre with 60% of fibre to resin ratio cured at room temperature is 130MPa (Elahi, Hossain, Afrin, & Khan, 2014). However, the maximum compression strength of the composite is 90MPa (CES Edupack, 2019). To avoid fatigue problems, the stress supported should never exceed the 50% of the maximum tensile strength so, the value used to compute the number of glass fibre layers will be 45MPa. From the design section, the geometry of the root wing is known, its chord is 300mm and it is 45mm thick. The minimum inertia of the section can be computed using the equation below:

$$I = \frac{M}{\sigma} \cdot y = \frac{4 \cdot 10^5 \text{ Nmm}}{45 \text{ MPa}} \cdot 22.5 \text{ mm} = 2.00 \cdot 10^5 \text{ mm}^4$$

The inertia of the root section is computed using an online free software (Online Wing Bending Inertia Calculator, 2019). Next, the value of the Inertia for a 2mm wall thickness:

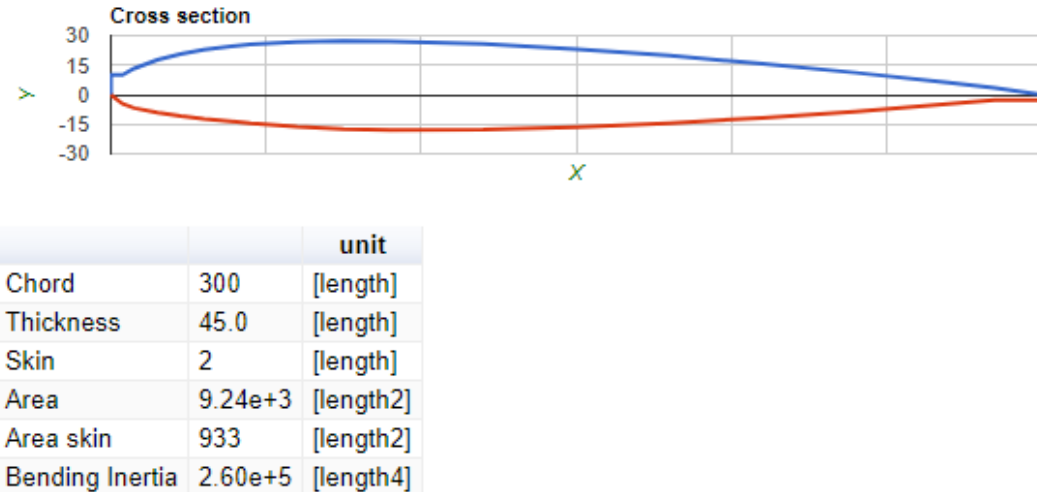


Figure 80: Naca 23015 bending inertia (Online Wing Bending Inertia Calculator, 2019)

The inertia is $2.6 \cdot 10^5 \text{ mm}^4$, but since the thickness is discrete, six layers of glass fibre were applied to both halves of the wing because either of them can be under compression. Six layers of fibre means 2.25mm wall thickness and this represents an inertia of $2.88 \cdot 10^5 \text{ mm}^4$. This represents a safety factor of: $\eta = \frac{I_{max}}{I} = \frac{2.88 \cdot 10^5}{2.00 \cdot 10^5} = 1.44$.

For the tail, the moment at the root is 67Nm, the chord and thickness are 180 and 22mm, so the inertia needed is:

$$I = \frac{M}{\sigma} \cdot y = \frac{6.7 \cdot 10^4 \text{ Nmm}}{45 \text{ MPa}} \cdot 11 \text{ mm} = 1.64 \cdot 10^4 \text{ mm}^4$$

The inertia of the tail with 4 layers each half would be $3.02 \cdot 10^4 \text{ mm}^4$ which would give a safety factor of: $\eta = \frac{I_{max}}{I} = \frac{3.02 \cdot 10^4}{1.64 \cdot 10^4} = 1.84$ which is a bit too high. However, since the lower part was made with 4 layers and 1.49mm skin thickness, the upper part was made with the same number of layers. The vertical stabilizer was also made with 4 layers of glass fibre each half which is also more than what is needed but it can resist better the possible hits it could have. One example of hit will be explained in the annex section.

5.2 Construction

The construction method used in this model has been an internal stainless-steel structure with fibre glass plastic reinforcement wings and wood and foam sandwich structure for the board. The construction will be separated in four different parts:

- Internal Structure: the internal stainless structure which have required arc soldering.
- Molds: the fusion 360 design and toolpath, the CNC machining and the post treatment to achieve good surface finish.
- Composite material skin: the lamination process using vacuum technology. Also, all the joints and final sanding of the parts.
- Board: the board construction which have to develop enough resistance and floatability.

5.2.1 Internal Structure

The joints of all the stainless-steel tubs have been done with arc soldering with 2mm electrodes of *Castolin* brand. To obtain a good surface contact and ensure resistance, all the circular unions needed a tip shape which matched the shape of the other tub. To avoid soldering deformation as much as possible, the perpendicular joints where always ensured with a machined to square plate of aluminium.



Figure 82: Welded joint



Figure 81: Ensuring perpendicularity with a machined to square aluminium plate

Also, shorter tubs were soldered in the points where the fiberglass parts need to be joined with the internal structure. This increments the surface of bounding and also allows glass fibre reinforced joints as later will be explained.



Figure 83: The results after the first welding day

The upper horizontal tub does not go underwater and can be square shaped. Its function is to rigidize the whole board. Two lateral tubs were also soldered to ensure that the surf board was properly attached to it. It is also important to notice that the two perpendicular joints were reinforced with diagonal tubs. The next image shows the finished internal structure with the tail already joined.



Figure 84: Finished internal structure

5.2.2 Molds

The elaboration of the molds is the most important part of the construction. They are responsible of the outer shape of the foil and must truly represent the geometry elaborated in the design section. Their surface finish will also have huge effect on the performance of the hydrofoil.



Figure 85: Finished wing mold

The first step is to design the molds in Fusion 360. To do so, there are some limitations that need to be considered. The CNC dimensions and the stock material used.

The maximum machining size, 500x500x120mm, is not big enough to machine the whole wing all at once because its span is 1m. to solve this problem, the wing mold needs to be divided in two parts. The stock material used in the elaboration of these molds was mdf. The reason is because its low price and its lack of wooden betas. It is also easy to machine and can be sanded until very good surface finish. However, the deepest section of the upper wing mold was 28mm. There were no thick enough mdf in the local store. So, two pieces of 16mm were glued together to form a 32mm thick piece of mdf. The glue used for the joints was wood glue from the brand Ceys. So, the stock material dimensions will be 500x500x32mm of mdf.

Once the stock is chosen, the Fusion 360 design can continue. The first operation was to separate the wing in four parts, the upper and lower section of each side. Then, the stock material was drawn as a 500x500x32mm square box. Next, the wing shape is cut from the box to obtain the final mold geometry. In Figure 86 a render of the shape which will be machined is shown.



Figure 86: Wing mold render

Now, all the 5 machining operations will be explained.

- Face: the face operation was used to obtain a flat surface and correct the possible deviations introduced when the piece was screwed to the CNC table. The stepover of each pass was 8mm and the cut was 1mm deep. Next, a photo of this operation is presented:

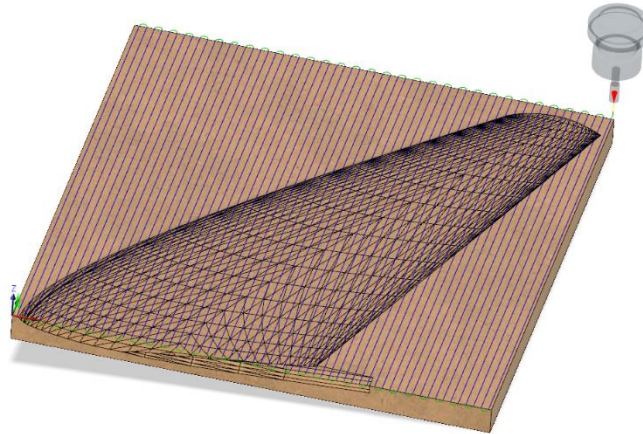


Figure 87: Face operation toolpath

- Adaptative clearing: this was the roughing operation, the responsible of the major material elimination. It consisted in making deep passes, 5mm, but with low tool load, 4mm. This allowed a bigger part of the tool flute to be in contact with the material and has reduced its tip wear. The finest passes of this operation leaved 1mm stairs. Next, a photo of the operation and another of the actual machining:

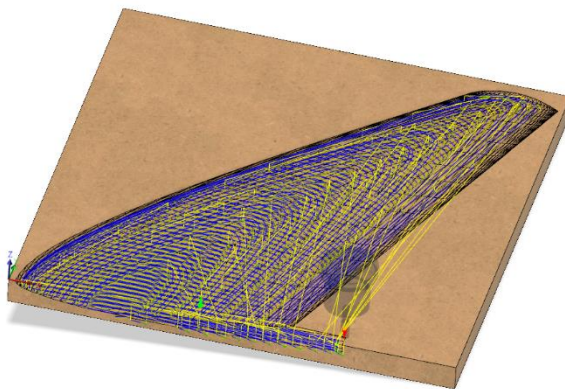


Figure 89: Adaptive clearing toolpath



Figure 88: Adaptive clearing machining

- Parallel: This was the finishing operation which leads the smoothest surface finish. It consisted on parallel passes separated 2mm between them. The direction of cut was parallel to the X axis. This has ensured a good finish on the leading and trailing edge. The following images shows the toolpath and the real cutting operation:

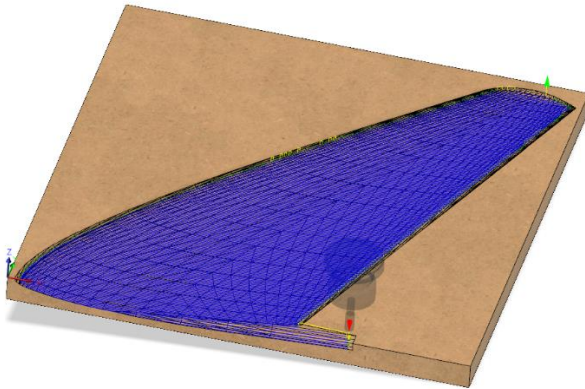


Figure 91: Parallel toolpath



Figure 90: Parallel machining

- Parallel 2: This operation was like the one explained before but 90 degrees shifted to finish the tub section where the fuselage is attached. This is shown in the following image:

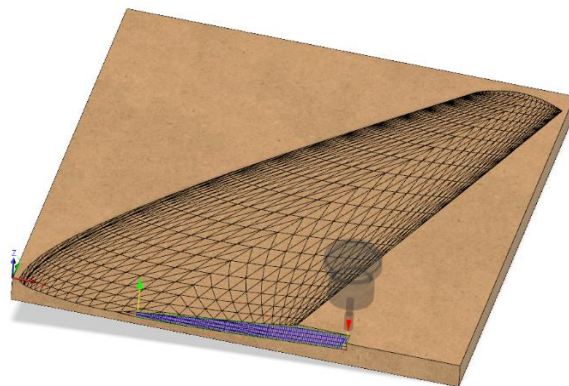


Figure 92: Parallel 2 toolpath

- Contour: this final operation is to clean the edges and ensure the perpendicularity of the face which will be joined with the other half. The passes were 2mm deep.

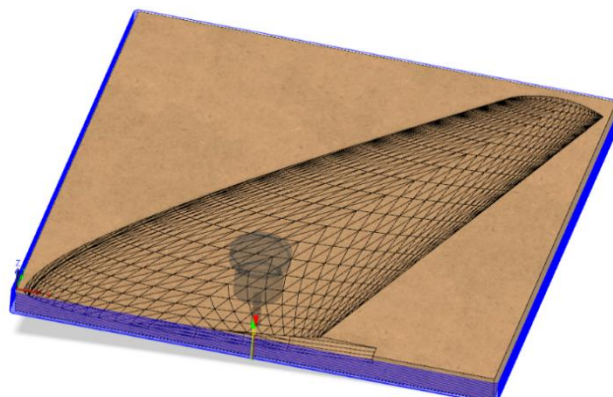


Figure 93: Contour toolpath

All the operations have been done at the maximum feedrate able for the machine, 3000mm/min. This is because the mdf needs a very high surface cutting speed, 195m/min and a chip load of 0.5mm with these values, the optimal feedrate needed would be 7500mm/min at 6200rpm as it is computed in the online feedrate fablab calculator (Fablab Speed and Feeds Calculator, 2019). If the surface cutting speed and the chip load are lowered to 160m/min and 0.3mm respectively, the obtained feedrate is 3000mm/min at 5000rpm. However, the rpm in this CNC machine cannot be known so they are adjusted until good chips are obtained.

The next step was to glue the molds together. To do so, wood glue and screws were used. After the glue had dried, the sanding began. The first attempt to sand the surface made clear that small fibres of the wood would never disappear because they were not rigid enough to be sanded. To solve this problem, all the surface was varnished with 4 layers of *mtn* brand spray varnish and then sanded again. This time, all the small fibres were rigid enough to be eliminated and a smooth glossy finish was accomplished. The sanding process started with 120 grid sand paper for the roughing sanding and ended with 400 grid paper for the smoothest finish. The next pictures show the difference finish quality before and after applying the varnish and sanding:



Figure 95: Surface finish before treatment



Figure 94: Surface finish after treatment

The last step of the molds preparation was the application of 4 layers of wax from *Liberon* brand. The wax ensures a good demolding and prevents the resin to stick to the mold. All the four layers were applied using a cotton cloth.

For the rest of the molds the process was exactly the same. They were a total of 7 pieces of wood machined. The time needed for machining the 4 wing parts was 1h 30min for each one, then 1h for each one of the tail and also 1h for the vertical stabilizer one. These 3 last pieces were able to be machined each at once, without gluing two finished molds. This was because the span of the tail was exactly 500mm. This made a total machining time of 9h but the preparation of each piece of wood took a lot of time in between.

The molds section ends here and some images of the final results are showed next.



Figure 96: Wing mold after varnishing



Figure 97: Finished tail mold

5.2.3 Lifting surfaces

It has been chosen to work with composite materials because is the actual technology and it presents an interesting challenge because of its extended applications once the technology is mastered. It can adopt almost any shape and, after curing the resin, the mechanical properties are very good. It can also be used under water without any major considerations apart from using the appropriated resin to do so. Despite the vanguard technology is carbon fibre reinforcement plastic, in this case glass fibre has been used. The reason is because the high price of the carbon fibre and the resin used with it. If the model had been made out of carbon fibre it could have been lighter but the mass of the glass fibre in comparison with the mass of all the surf board, rider included, represents a very low percentage and does not compensate the cost increase.

The fibre bought to build this model was 10m² of 300gr/m² chopped mat glass fibre. This mat has short fibres, about 100mm each, randomly distributed along the cloth. Its mechanical properties are lower than the ones of fabric cloths where the fibres are woven but, again, the price of woven fabrics is much higher and the weight reduction does not compensate the cost increase, for this project. The resin used is Polyester isophthalic which is adequate for naval usage (Nazza, 2019). For this job, 2kg of this type of resin were at disposal with its respective hardener, methyl ethyl ketone peroxide; which is mixed in a 2.5% mass ratio with the polyester resin.

The methodology used to elaborate all the fibre parts is vacuum forming. This consists in using the atmospheric pressure to compress all the fibre layers against the mold, ensuring that the cloth adopts the desired shape and also extracts all the excess resin. The order of the different layers is: the mold, the demolding agent, the impregnated composite, a perforate film of polyethylene which does not stick to the resin and allows the resin excess to pass through, some paper to absorb the resin excess and, lastly, the vacuum bag. The air inside the vacuum bag is extracted using a vacuum pump which was extracted from an old fridge.



Figure 99: Vacuum fridge pump



Figure 98: Perforated polyethylene film

The first part elaborated was the lower half of the tail. This part would be used as a first trial to know which is the thickness obtained in relation with the number of layers and the fibre to resin weight ratio.

The first step was to elaborate a template to cut the fibre. To elaborate this template, a paper sheet was pressed to suit the mold and then it was marked and cut. Then, this template was transferred to the glass fiber mat and cut using a cutter. For this first attempt, 4 layers of glass fiber were used, which had a total weight of 95g.



Figure 101: Paper template



Figure 100: Template transferred to the fibre mat

The second step was to prepare the vacuum bag. A layer of plastic film was placed under the mold and double-sided tape was added to the perimeter. To attach the vacuum tube to the bag, a 3d printer adapter was designed. This piece had a flat surface where a big strap of double-sided tape could be bounded and a hole to let the air pass through. Next, a photo of the adapter is presented.



Figure 102: Plastic adapter for the vacuum tub

The third step was to prepare and lay the composite material. For this case, 200 g of resin were mixed. Then, each layer was collocated on the mold and impregnated with resin using a roller, which also was used to extract big air bubbles and ensure a good positioning of the cloth.



Figure 103: Manual-laying the composite material

Finally, the perforated film was laid over the last coat of resin and over it, the absorbing paper. Then, the vacuum bag was fully closed by bounding another layer of plastic film with the double-sided tape before located. Then, the vacuum pump started to suck all the air inside. A very important step is to press the vacuum bag while the pump is on to avoid the phenomena called bridging, which consists in the fibre not reaching small concavities. Some pictures of this process are presented next.



Figure 105: Pressing the vacuum bag to avoid bridging



Figure 104: Resin excess being absorbed by the paper

The demoulding process required a spatula but it came out relatively easy. This was the piece just after extracting it from the mold:



Figure 106: First composite part



Figure 107: Checking the wall thickness

The mass of the cured part was 164g and the mass of fibre used was 95g. This means that the fibre to resin weight ratio obtained through this methodology is 58%. Also, the thickness of the four layers composite was 1.49mm as it can be seen in the Figure 107. These two values are very important because they allow to search for information about the properties and the required layers needed to withstand the loads. These results mean that every layer of glass fibre will increase the thickness in average 0.375mm.

All the other parts were developed following the same procedure. The number of layers for each part is chosen in the before explained 5.1.2 Lifting surfaces.

Once the 6 halves of the 3 lifting surfaces were done, it was time to joint them with the internal stainless-steel structure. A very important consideration was that all the pieces were aligned as they should. To do so, the upper half was placed at its correct position, which was measured with a level, and then it was glued with the same 5 min epoxy glue used to glue the plastic parts in Figure 46. Then, strips of glass fibre were laid over the metal tubs, that were previously soldered, ensuring a resistant bond between the composite parts and the stainless-steel structure. The reason of choosing the upper half to be glued to the internal structure was because is the one that is suctioned away from the structure, instead, the lower one is compressed upwards. Some photos are now shown:



Figure 108: Leveling the tail



Figure 109: Wing joint procedure



Figure 110: Tail joint procedure

After the upper halves were bounded to the metal structure, the other halves needed to be joined. As it can be seen in the image below, the trailing edge joint has enough gluing surface and can be joined without major problems. However, the leading edge has very small surface and cannot be joined only with glue.

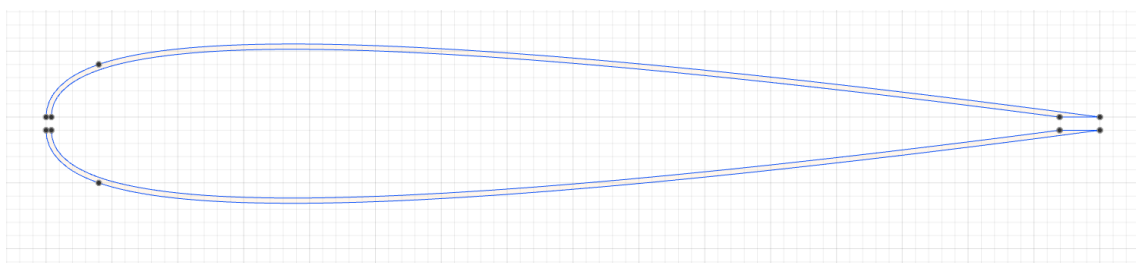


Figure 111: Joint surface problem

To solve this problem, it was necessary to increase the bounding surface. To do so, the best solution was to add a fiberglass strip all around the leading edge to obtain this type of joint:

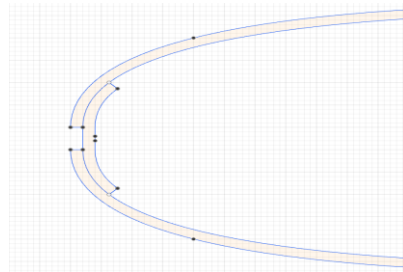


Figure 112: Joint solution

This solution does not only increment the bounding surface it also changes the pulling angle and now the glue is working at shear stress which is better than tensile. In order to not influence the design geometry, the joint must be in the inner part. This leads in the problem that once the other half is put on top, there is no way to control if the strip is in the middle of the joint. To solve this problem, the glass fibre strip was bounded only with the lower part, leaving the upper section of the strip without resin. Once the half strip resin was dried, the reinforcement was locked. At this point, it was possible to apply resin to the other half and accommodate the other wing half over. To maintain its position, clamps were used in the leading edge and clothespins in the trailing edge.



Figure 113: Leading edge fibre strip



Figure 114: Clamping the halves

The next step was to fill the inner cavity with polyurethane insulation spray foam. To do so, the spray cannula was inserted through a small hole. Once there, the application began. As this type of spray expands and adopts any shape, only one application point was needed. Because of the slightly translucence of the fibre glass, the progress of the foam could be visualised and the complete fulfil confirmed.

Finally, the excess of foam was sanded using sand paper 120 grid and the fibre excess of the joints was eliminated using an angular grinder. Some photos of the final result are now shown:



Figure 116: Polyurethane foam fill



Figure 115: Final result after sanding

5.2.4 Board

The principal objectives of the board are to provide floatability and a rigid surface where the rider can stand on. As it has been done with the scale board, the explanation will be found in the Annex section.

Finally, the real scale model was complete.



Figure 117: Finished prototype

5.3 Tests

The following tests were all done with a boat acting as a tug. This has allowed the tests to be replayed many times a day without needing surf skills, without meteorological dependence and having an accurate control over the speed.

5.3.1 First test

The first test was done on 19th of May and the director Aleix Báez was present. The way the board was pulled was using a rope that the rider had in his hands. The first tries seemed that the tugboat was too slow because the foil was not producing enough lift and the engine was at full throttle, at 6.5knts, which is 3.2m/s. After a few tries, the lower wood of the board was decoupled and also the lower foam. To correct this, a rope was rounded around the board to be able to continue with the tests. The flat tip was also not helping because it was getting inside the water and lifting up water to the rider's face which was very uncomfortable. But suddenly, when the rider moved its body backwards delaying the centre of mass position, the hydrofoil began lifting and taking off the water. The first time was a very short flight because the wing got off the water but after a few tries the rider realised that for taking off the body needed to be moved backwards but once it was off the water the centre of mass needed to be advanced again to maintain a stable flight. In this occasion the only tried position was with the belly resting over the board. In addition, the force needed to start the flight when the board was yet on the water was very high and tiring for the rider, however, when the foil came out of the water the force required to maintain the speed was way lower. The following photo was taken at the last flight which was about 15s long and ended when the left wing got off the water and lost all of its lift.



Figure 118: First test

5.3.2 Second test

The second test was made with a much faster boat. However, the speed did not seem to solve the poor lift problem. Instead, much more pulling force was needed to maintain a 10knts take off and the rider get tired much faster. To avoid the fatigue, the rope was passed a few times throw the door handle attached to the board. This made possible to adopt a different position, with the knees on the board. In this new position, the centre of mass can be moved more easily and ended up with a much longer and controlled flight. Once again, the ability to change the mass position is what made possible to accomplish a successful flight. This means that a stand position should be better for controlling the board. Unfortunately, the tension needed in the arm and the slippery wood made not possible for the rider to stand over the board. The next photo shows the knee position in a successful flight.



Figure 119: Second test

5.3.3 Third test

This test was again developed with the slower boat. The modifications for this test were the addition of a non-slippery surface but the most important one was that the pulling rope was attached directly to the board, which made possible for the rider to only worry about his equilibrium with the help of a rope attached to the door's handle. Not only the stand-up position was possible with this configuration, it also was much easy to control and the flight was possible even at 4knts, however, lower than 5knts was much difficult to sustain. The flights duration was not a problem anymore. However, an important point is that the instabilities came from sideways movements, roll instability, not from longitudinal. The position was difficult to recover when the board tilted to one side. Contrary, the pitch angle was easy to change and maintain at will. This was the most successful test and the one with longest and most controlled flights. The next photo shows the stand-up position.



Figure 120: Third test

6. Future work

There are three tasks to do as an extension for this project:

- Validate the Simulink platform: to do so, more cases should be studied and compared with the tests results. However, the tests should also allow data recovery to not being only qualitative.
- Use the hydrofoil to surf waves: for this future task, a professional surfer would be needed. The tests have shown that the board is stable enough to stand on and it should be possible to ride waves with the appropriated skills. From this point, a geometry modification may be introduced in order to obtain the appropriated balance between stability and manoeuvrability.
- Construction techniques: It must be noted that prototyping tools were used for the manufacturing of the hydrofoil. A future improvement could be the mass production to reduce the manufacturing costs and time.

7. Timing

The schedule for this project has been followed and the work did not stop from the first day. The prove of it is that the proposed day for the first scale test in the Gantt diagram of the project charter was on 1st of April and the first test was developed on 11th of the same month, just 10 days later. Something similar happened with the first real scale test, the assigned day was on 13th of May and the actual test was done on 19th of the same month, just one week late. The following image is the Gantt diagram posted on the project charter:

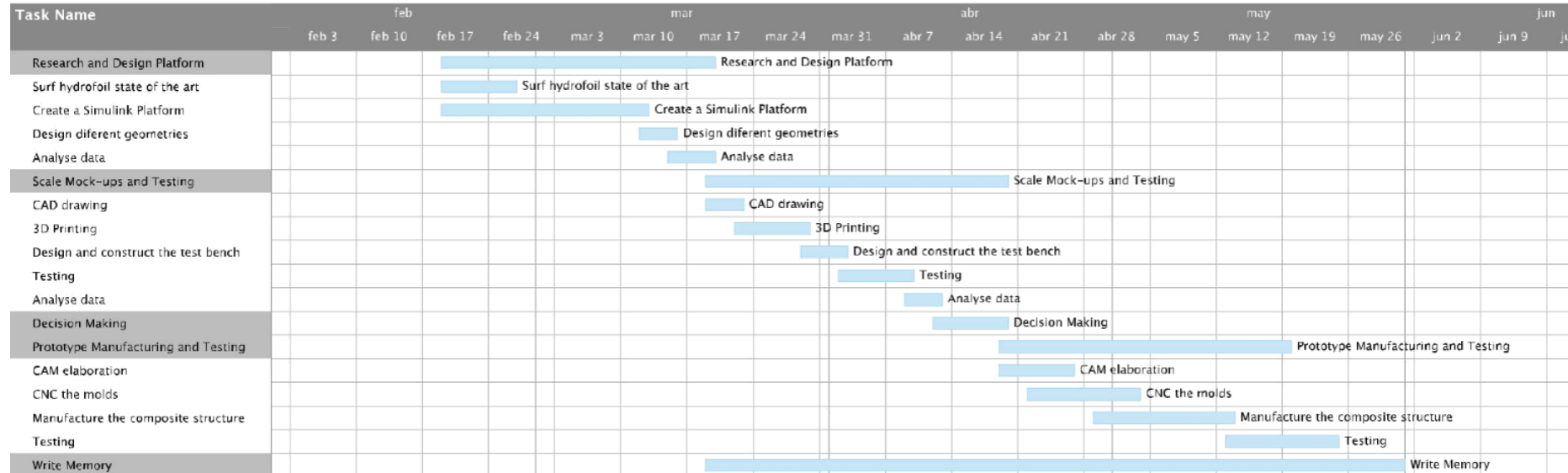


Figure 121: Project charter's Gantt diagram

8. Conclusions

This project has recreated the typical industry challenge. There was a list of objectives that need to be accomplished within a deadline, a budget and the tools and machines available. The whole process has passed through a design stage, tests to validate the geometry designed and the software implemented and a final real prototype.

The design section has shown that the principal problem of a hydrofoil surf is its centre of mass height, which forces the need of a very stable plane. The static stability was achieved by iterative design using the Open VSP and the dynamic stability was evaluated with an own designed Simulink platform. The results from the platform were similar to the obtained on the tests, however, the software predicted a higher flight speed than the actually needed.

In the scale model section, two geometries were 3d printed and tested in the test bench. Overall, the conventional design was the one with better performance. This fits with the actual technology used on hydrofoils since all of them have the same distribution of lifting surfaces. The results obtained from the tests match with the ones obtained via Simulink platform which means the platform could be used for future design iterations.

Finally, in the real scale model construction, the structure was designed and constructed using composite materials and currently state of the art technology. The pulling tests have shown that the geometry is stable and a beginner was able to ride the board without major problems; thus accomplishing the most important of the objectives.

Overall, this project has presented a list of challenges which have all been overcome to end up with a functional hydrofoil that could be used to ride waves and all of this was done in a regular house, for a non-professional student and with own constructed machines.

9. Bibliography

- Acosta, A. J. (1973). *Hydrofoils and Hydrofoil Craft*. Pasadena, California: California Institute of Technology. Retrieved from <https://authors.library.caltech.edu/316/1/ACOarfm73.pdf>
- Airfoil Tools. (2019, March). Retrieved from <http://airfoiltools.com/>
- Arduino Forum. (2019, April). Retrieved from <https://forum.arduino.cc/index.php?topic=579183.0>
- Azo Materials. (2019, Mayo). Retrieved from <https://www.azom.com/article.aspx?ArticleID=8211>
- B3 Proshop. (2019, Febrero). Retrieved from <https://www.b3proshop.com/es/>
- Basic Aircraft Design Rules. (2019, March). Retrieved from <https://ocw.mit.edu/courses/aeronautics-and-astronautics/16-01-unified-engineering-i-ii-iii-iv-fall-2005-spring-2006/systems-labs-06/spl8.pdf>
- CES Edupack. (2019, Mayo). Retrieved from <https://grantadesign.com/teachingresource/material-science/>
- Eisenberg, P. (1968). *Cavitation*. Massachusetts: MIT. Retrieved from <http://web.mit.edu/hml/ncfmf/16CAV.pdf>
- Elahi, A. F., Hossain, M. M., Afrin, S., & Khan, M. A. (2014). Study on the Mechanical Properties of Glass Fiber Reinforced Polyester Composites. *International Conference on Mechanical, Industrial and Energy Engineering*, (p. 5). Khuina, Bangladesh.
- Fablab Speed and Feeds Calculator. (2019, Abril). Retrieved from https://pub.pages.cba.mit.edu/feed_speeds/
- Franchini, S., & López, O. (2011). *Introducción a la Ingeniería Aeroespacial*. Madrid: Garceta Grupo Editorial.
- Gómez, M. A., & Pérez, M. (2012). *Mecánica de Vuelo*. Madrid: Garceta Grupo Editorial.
- Human Benchmark. (2019, Marzo). Retrieved from <https://www.humanbenchmark.com/tests/reactiontime>
- Nazza. (2019, April). Retrieved from https://www.nazza.es/img/cms/documentos%20PDF/Fichas%20T%C3%A9cnicas/FT-resina-de-poliester-isofthalica_1.pdf
- Online Wing Bending Inertia Calculator. (2019, Mayo). Retrieved from http://www.wingbike.nl/Wingbike_Hydrofoil/Airfoil_bending_inertia.html
- Strian. (2019, Mayo). Retrieved from <http://structural-analyser.com/>
- Wikipedia Bending. (2019, Mayo). Retrieved from <https://en.wikipedia.org/wiki/Bending>
- Wikipedia Second Moments of Inertia. (2019, Mayo). Retrieved from https://es.wikipedia.org/wiki/Anexo:Momentos_de_inercia_de_%C3%A1reas

